A&A 526, A148 (2011)
DOI: 10.1051/0004-6361/201015302

Astronomy & Astrophysics

Dying radio galaxies in clusters

M. Murgia[1], P. Parma[2], K.-H. Mack[2], H. R. de Ruiter[2], R. Fanti[2], F. Govoni[1], A. Tarchi[1], S. Giacintucci[3], and M. Markevitch[3]

[1] INAF – Osservatorio Astronomico di Cagliari, Loc. Poggio dei Pini, Strada 54, 09012 Capoterra (CA), Italy
e-mail: matteo@oa-cagliari.inaf.it
[2] INAF – Istituto di Radioastronomia, via Gobetti 101, 40129 Bologna, Italy
[3] Harvard-Smithsonian Center for Astrophysics, 60 Garden St., Cambridge, MA 02138, USA

Received 30 June 2010 / Accepted 29 October 2010

ABSTRACT

Aims. We present a study of five "dying" nearby ($z \leq 0.2$) radio galaxies belonging to both the WENSS minisurvey and the B2 bright catalogs WNB1734+6407, WNB1829+6911, WNB1851+5707, B2 0120+33, and B2 1610+29.
Methods. These sources have been selected on the basis of their extremely steep broad-band radio spectra, which strongly indicates that either these objects belong to the rare class of dying radio galaxies or we are observing "fossil" radio plasma remaining from a previous instance of nuclear activity. We derive the relative duration of the dying phase from the fit of a synchrotron radiative model to the radio spectra of the sources.
Results. The modeling of the integrated spectra and the deep spectral index images obtained with the VLA confirmed that in these sources the central engine has ceased to be active for a significant fraction of their lifetime, although their extended lobes have not yet completely faded away. We found that WNB1851+5707 is in reality composed of two distinct dying galaxies, which appear blended together as a single source in the WENSS. In the cases of WNB1829+6911 and B2 0120+33, the fossil radio lobes are seen in conjunction with a currently active core. A very faint core is also detected in a MERLIN image of WNB1851+5707a, one of the two dying sources composing WNB1851+5707. We found that all sources in our sample are located (at least in projection) at the center of an X-ray emitting cluster.
Conclusions. Our results suggest that the duration of the dying phase for a radio source in a cluster can be significantly higher than that of a radio galaxy in the field, although no firm conclusions can be drawn because of the small number statistics involved. The simplest interpretation of the tendency for dying galaxies to be found in clusters is that the low-frequency radio emission from the fading radio lobes lasts longer if their expansion is somewhat reduced or even stopped. Another possibility is that the occurrence of dying sources is higher in galaxy clusters. We argue that radio sources in dense environments, such as the center of cooling core clusters, may have a peculiar accretion mode which results in a bursting duty cycle sequence of active and quiescent periods. This result could have important implications for theories of the life cycles of radio sources and AGN feedback in clusters of galaxies but awaits confirmation from future observations of larger, statistically significant, samples of objects.

Key words. radio continuum: galaxies – galaxies: active – galaxies: clusters: general

1. Introduction

Dying radio galaxies represent an interesting, but still largely unexplored, stage of the active galactic nuclei evolution. During their active stage, which may last several 10^7 years, the strong radio sources associated with elliptical galaxies are supplied with energy from active galactic nuclei via plasma beams or jets. Owing to the continuous accumulation of new particles, the total spectra of the active radio sources are usually well approximated by a power law over a wide range of frequencies. The injection of energy also sustains the growth of these radio sources that is governed by the balance between the internal pressure in the radio lobes and the pressure in the hot X-ray emitting external medium into which they must expand (Scheuer 1974).

At some point, however, the activity in the nuclei stops or falls to such a low level that the plasma outflow can no longer be sustained and the radio source is expected to undergo a period of fading (dying phase) before it disappears completely. In the dying phase, the radio core, well-defined jets, and compact hotspots will disappear because they are the structures produced by continuing activity. On the other hand, the radio lobes may still remain detectable for a long time if they are subject only to radiative losses of the relativistic electrons. The first example of such sources was B2 0924+30, which was illustrated by Cordey (1987). It is also possible that radio galaxies may be active intermittently or even that jets flicker before eventually going off completely. In this scenario, one expects to observe fossil radio plasma remaining from an earlier active epoch, along with newly restarting jets. The best case of fossil radio lobes seen with a currently active galaxy is 3C 338 (see e.g. Gentile et al. 2007). The very steep spectrum lobes of this source are clearly disconnected from the currently active jets.

We classify a radio source as dying not only if the fossil lobes are detached from the AGN and there is no evidence of nuclear activity (trivial case), but also if some kind of nuclear activity is present but the fossil lobes still dominate the total source's radio luminosity[1]. Hence, in what follows we refer to both dying and

[1] This choice is motivated by the following two considerations. First, even if the nuclear component we are observing is really produced by a new couple of restarting radio jets, we would never know a priori if this new activity would be able to last enough to regenerate a radio galaxy similar to the previous event of radio activity of which the fossil lobes represent the remains. Second, it may be not obvious to recognize whether a nuclear component is produced by the start of a new phase of AGN activity or it is rather a fading radio core that is definitely turning-off.

re-starting sources if the fossil lobes are the dominant component. We suggest instead to reserve the term *renewed source* to indicate the case in which the new and the fossil components are roughly comparable in luminosity, as in the case of the double-double radio sources (Schoenmakers et al. 2000; Saripalli et al. 2002, 2003).

Given the comparatively short duration of the radio galaxy phenomenon, we could expect a large number of dying radio sources. However, only a handful of dying radio galaxies in this evolutionary stage are known. According to Giovannini et al. (1988), only a few percent of the radio sources in the B2 and 3C samples have the characteristics of a dying radio galaxy. We note that these sources represent the last phase in the "life" of a radio galaxy. Therefore they must be well distinguished from the cluster radio halo/relic phenomenon, which is usually not associated with an individual galaxy (see Ferrari et al. 2008, and references therein).

A possible explanation of the rarity of the dying radio galaxies may be their relatively fast spectral evolution during the fading phase. Synchrotron losses and the inverse Compton scattering of the cosmic microwave background photons preferentially deplete the high-energy electrons. The fading lobes are expected to have very steep ($\alpha > 1.3$; $S_\nu \propto \nu^{-\alpha}$) and convex radio spectra characteristic of an electron population that has radiated away much of its original energy (Komissarov & Gubanov 1994). In the absence of fresh particle injection, the high-frequency radio spectrum develops an exponential cutoff. At this point, the adiabatic expansion of the radio lobes concurs to shift this spectral break to lower frequencies and the source quickly disappears. On the other hand, if the source expansion is somehow reduced, or even stopped, the fossil radio lobes may still be detected, at least at low frequency.

For the reasons mentioned above, low-frequency selected samples such as the Westerbork Northern Sky Survey (WENSS; Rengelink et al. 1997) at 325 MHz and the B2 survey at 408 MHz (Colla et al. 1970, 1972, 1973) are particularly well-suited to searching for these elusive fossil radio sources. Parma et al. (2007), by cross-correlating WENSS and NVSS (Condon et al. 1998), discovered six new dying sources and three new restarted sources. Another two dying galaxies (the central radio source in Abell 2622 and MKW03s) and one possibly restarting source (MKW07) were found by Giacintucci et al. (2007) in a low-frequency survey of nearby cluster of galaxies performed with the Giant Metrewave Radio Telescope.

In this paper, we report on a search for dying sources in a WENSS sub-sample (the minisurvey; de Ruiter et al. 1998) and the B2 bright sample described by Colla et al. (1975). Both samples were constructed from the parent surveys by identifying the radio sources with nearby bright galaxies. From these samples, we selected five dying radio galaxy candidates whose extremely steep spectra are characterized by a quasi-exponential drop above a frequency of about 1 GHz. These are WNB1734+6407, WNB1829+6911, WNB1851+5707, B2 0120+33, and B2 1610+29.

To determine whether these sources are really dying objects or fossil lobes associated with restarting radio galaxies, we studied their radio continuum emission with the Very Large Array (VLA) at various frequencies. Our new observations and the analysis of the data already available in literature permitted us to derive detailed integrated radio spectra and spatially resolved spectral index images for all the five candidates. We were also able to observe at sub-kpc resolution the source WNB 1851+5707 with the Multi-Element Radio Linked Interferometer Network (MERLIN) interferometer. Furthermore, we found that all the five sources are unambiguously associated with diffuse X-ray emission in the Rosat All Sky Survey (RASS). In all cases, the association is with a known cluster of galaxies.

We report the results of this extensive campaign of radio observations. In Sect. 2, we described the criteria of source selection. The descriptions of the VLA and MERLIN observations are reported in Sects. 3 and 4, respectively. In Sect. 5, we present our analysis of the radio spectra. The X-ray environment is presented in Sect. 6. Finally, a summary of the work is given in Sect. 7.

Throughout this paper, we assume a ΛCDM cosmology with $H_0 = 71$ km s^{-1} Mpc^{-1}, $\Omega_m = 0.3$, and $\Omega_\Lambda = 0.7$.

2. Source selection

2.1. The spectral curvature of dying and restarting sources

In the active stage, the total spectra of the radio galaxies are usually approximated well by a power law over a wide range of frequencies. Spectral breaks at high frequencies are also often observed. The break frequency is due to the radiative losses of the synchrotron electrons and can be related to the magnetic field and age of the source. If the integrated spectrum of the radio source is dominated by the emission of the radio lobes, which accumulate the electrons injected by the jets, it can be modeled by a continuous injection model (CI) in which the low-frequency spectral index $\alpha_{\rm low}$ represents the injection spectral index of the youngest electron populations, $\alpha_{\rm inj}$, while the high-frequency spectral index is limited to $\alpha_{\rm high} \leq \alpha_{\rm inj} + 0.5$ at frequencies greater than the break frequency (see e.g. Murgia et al. 1999). As the source ages, the break moves to lower frequency and the radio spectrum eventually becomes a steep power law in which $\alpha_{\rm low}$ approaches $\alpha_{\rm high}$. For dying sources however, we expect to find an exponential cut-off of the integrated spectrum above the break frequency (e.g. Parma et al. 2007). In this case, the high-frequency spectral index, $\alpha_{\rm high}$, may became much steeper than the low-frequency one, $\alpha_{\rm low}$. On the other hand, if the activity in the galaxy nucleus restarts $\alpha_{\rm high}$ can be flatter that $\alpha_{\rm low}$. A possible selection criterion may then be based on the radio spectrum curvature to distinguish active, dying, and restarting sources. Following the idea of Sohn et al. (2003), we define the spectral curvature[2], *SPC*, as

$$SPC = \alpha_{\rm high} - \alpha_{\rm low}. \quad (1)$$

For the optically thin portion of the radio spectrum, in the framework of the CI model the spectral curvature will be very close to $SPC \approx 0$. The maximum curvature we could expect in the active phase is indeed limited to $\alpha_{\rm high} - \alpha_{\rm low} \leq 0.5$.

On the other hand, the integrated spectra of dying sources are characterized by an exponential cut-off at high frequencies, thus for them extreme spectral curvatures ($SPC \gg 0.5$) are possible. Finally, for restarting sources the injection of new electrons will flatten the high frequency spectrum resulting in $\alpha_{\rm high} < \alpha_{\rm low}$, and thus $SPC < 0$ (Murgia, in preparation).

The proposed spectral curvature classification must obviously always be considered to have a statistical meaning and used by taking into account the following caveats and warnings. The *SPC* to be meaningful should be calculated over a broad frequency range. Because of the nature of the synchrotron radiation, the spectral curvature of integrated spectra generally occurs over a frequency range of at least two order of magnitudes.

[2] Please note that Sohn et al. (2003) adopted a slightly different definition of *SPC* than the one proposed here.

Table 1. Basic properties of the dying radio galaxy candidates.

Source	RA (J2000) (h m s)	Dec (J2000) (d m s)	Redshift	Scale (kpc/″)	$S_{325\ \mathrm{MHz}}$ (mJy)	$\alpha_{1.4\mathrm{GHz}}^{325\mathrm{MHz}}$	*SPC*
WNB1734+6407	17 35 04.6	+64 06 07.7	0.1406	2.4	120	2.0	1.1
WNB1829+6911	18 29 05.6	+69 14 06.0	0.204	3.3	209	1.9	-0.4
WNB1851+5707a	18 52 08.5	+57 11 42.3	0.1068	1.9	368	1.7	1.1
WNB1851+5707b	18 52 09.7	+57 11 56.6	0.1066				
B2 0120+33	01 23 39.9	+33 15 22.1	0.0164	0.33	727	1.3	1.5
B2 1610+29	16 12 35.5	+29 29 05.3	0.0318	0.63	412	0.9	0.8

Notes. Spectral indices and flux densities are from the WENSS and NVSS. The spectral curvatures are calculated by measuring α_{low} between 151 and 325 MHz, for the WENSS minisurvey sources, and between 151 and 408 MHz, for the B2 sources. The high-frequency spectral index α_{high} is taken between 1400 and 4850 MHz for all sources.

Hence, if the observed spectral range is too narrow, there is always the possibility of misclassifying as active a radio galaxy that is instead dying. Re-starting sources are particularly problematic from this point of view because, as the injection of new radio plasma proceeds, the spectral curvature of the source eventually decreases from $SPC > 0.5$ to $SPC < 0$, so all values of *SPC* are in principle possible for them (see Sect. 2.3 for the case of 3C 338). Moreover, individual radio sources could not fit into the above picture if their integrated spectrum is dominated by Doppler-boosted components, such as jets, flat spectrum cores, etc. Other common problems in radio surveys, e.g. the blending of unrelated sources or the difficulties in imaging extended sources, could lead to spurious *SPC*. For all these reasons, the final confirmation of a dying source requires follow-up observations of deep, spatially resolved, spectral-index radio imaging of the dying candidate.

With this strategy in mind (*SPC* selection and deep spectral index imaging), we searched for dying and restarting sources candidates in two samples extracted from the WENSS and the B2 catalogs.

2.2. The WENSS minisurvey sample

Dying radio galaxies are more easily detected at low frequency, hence the WENSS at 325 MHz is particularly well-suited to searching for these elusive objects. We are interested in steep-spectrum radio sources identified with bright galaxies as these should be prime candidates for dying sources (Parma et al. 2007). The WENSS minisurvey contains 402 radio sources identified with either elliptical or spiral galaxies with red magnitudes brighter than roughly $m_{\mathrm{r}} = 17-18$. Using cross-correlation with the existing catalogs and new observations with the Effelsberg 100-m telescope at 4.8 and 10.4 GHz (Mack et al., in prep.), we obtained spectral information in the frequency range from 38 MHz to 10 GHz for about 200 sources brighter than $S_{325} > 30$. The spectral curvature can be used to select dying radio galaxy *candidates* in large samples, as in the minisurvey, where detailed high-resolution images are not available but there is a good spectral coverage.

Three of these 200 sources show a quasi-exponential drop of their integrated spectrum with a spectral index as steep as $\alpha > 1.5$ at 1.4 GHz. These sources are WNB1734+6407, WNB1829+6911, and WNB1851+5707.

The spectral curvatures, calculated between 151 and 325 MHz (for α_{low}) and between 1400 and 4850 MHz (for α_{high}), for the three sources are, respectively, $SCP = 1.1, -0.4$, and 1.1. Thus, WNB1734+6407 and WNB1851+5707 can be classified as dying source candidates, while WNB1829+6911 would be a restarting source candidate.

All three radio sources are associated with elliptical galaxies (see Table 1 for a list of their basic properties). As we show in the next section, WNB1851+5707 is indeed composed of two distinct dying galaxies that are blended together in the WENSS. The two redshifts listed in Table 1 were obtained with the DOLORES spectrograph installed at the 3.5-m Galileo telescope on the Roque de los Muchachos in La Palma, Spain (see Parma et al. 2007, for more details about the optical photometry).

To determine whether these sources were really dying objects or relic lobes associated with active radio galaxies, we observed their continuum emission in detail with the VLA. The brighter and more compact of the three, WNB1851+5707, was also observed with MERLIN.

2.3. The B2 sample

The B2 bright sample described in Colla et al. (1975) has been selected with very similar criteria to the WENSS minisurvey: radio sources with a flux density >200 mJy at 408 MHz were identified with bright nearby galaxies. This complete sample consists of 54 elliptical galaxies, thus we may expect it to contain a few dying sources. For the B2 sample, detailed VLA images are available. We searched for sources with relaxed radio morphologies and extreme spectral curvatures mostly calculated between 151 and 408 MHz (for α_{low}) and between 1400 and 4850 MHz (for α_{high}). The prototypical dying source B2 0924+30 with $SPC = 0.8$ and the restarting source[3] 3C338 (alias B2 1626+39) with $SPC = 0.7$ belong to this sample.

We searched for dying or re-starting source candidates to complement B2 0924+30 and B2 1626+39. We found that the radio sources B2 0120+33 and B2 1610+29, with a spectral curvature of $SPC = 1.5$ and $SPC = 0.8$, respectively, can indeed be considered dying radio source candidates. The radio source B2 0120+33 is associated with the elliptical galaxy NGC 507 at the center of the Zwicky Cluster 0107.5+3212. The source has a weak radio core and its large scale radio emission appears very faint and diffuse at a resolution of a few arcseconds even at 1.4 GHz (Parma et al. 1986). The second candidate, B2 1610+29, is associated with the nearby cD central galaxy NGC 6086 in Abell 2162 and has a relaxed morphology in the VLA 1.4 GHz image of Parma et al. (1986). The source was

[3] Note that in this restarting source the active core-jet component accounts for just a small fraction of the source's flux density, which is dominated by the steep spectrum lobes in the considered frequency window.

imaged with the GMRT at 610 MHz by Giacintucci et al. (2007), who found a very similar morphology.

By using all the useful data that have been made available in the VLA archive since then, we studied in detail the spectral properties of these objects to determine whether they really are dying sources.

3. VLA observations and data reduction

3.1. New observations

We observed the three dying radio galaxy candidates from the WENSS minisurvey at 1.4 and 4.8 GHz with VLA in various configurations. A summary of this campaign of observations, including the VLA configuration, frequency, date, and length of observations, is reported in Table 2. A bandwidth of 50 MHz was used for each of the two frequencies.

Calibration and imaging were performed with the Astronomical Image Processing System (AIPS) following the standard procedure of Fourier-transform, clean and restore. Self-calibration was applied to remove residual phase variations. Data from different arrays were combined to improve uv-coverage and sensitivity. We combined the A, B, and C arrays at 1.4 GHz and the C and D at 4.8 GHz. Each combined data set was self-calibrated. The relevant image parameters are reported in Table 3.

To estimate the flux density and the spectral index of the three sources, the primary beam correction was applied to all the images by applying the AIPS task PBCOR. For the purposes of the spectral index imaging, we convolved the 1.4 GHz images to the slightly larger beam of the 4.8 GHz ones. However, we emphasize that the angular resolution of the final images at the two frequencies were already well matched, not just by filtering the data, but by having comparable intrinsic coverage over the relevant spatial frequencies. Furthermore, both data sets have nearly the same sensitivity levels.

The VLA total intensity iso-contours of WNB 1734+6407, WNB 1829+6911, and WNB 1851+570 at 1.4 and 4.8 GHz are shown, respectively, in the top left and right panels of Figs. 1 to 3. The 1.4 GHz contours are overlaid on the optical image of the red Digital Sky Survey (DSS2), while the 4.8 GHz contours are overlaid on the spectral index image between the two radio frequencies.

3.2. Archival data

We recover from the VLA archive all useful data available for the radio sources B2 0120+33 and B2 1610+29. A summary of relevant parameters of the images produced is provided in Table 3.

The source B2 0120+33 has a useful 325 MHz B-array observation in the VLA archive (project AC0845). The observation was acquired in line mode with 15 spectral channels in a 6 MHz bandwidth for each of the two IFs. The source 3C 48 was used as amplitude, phase, and bandpass calibrator. In the final imaging, the data were averaged to six channels and mapped using a wide-field imaging technique, which corrects for distortions in the image caused by the non-coplanarity of the VLA over a wide field-of-view. A set of overlapping fields was used to cover an area of about $2.5^\circ \times 2.5^\circ$ around the radio source. All these fields were included in CLEAN and used for several loops of phase self-calibration. The central frequency of the final images is 324 MHz. At 1.4 GHz we produced a B+C image at a resolution of about 10″. This image is shown in the top-left panel of Fig. 4. The resolution of the C array 1.4 GHz image alone closely matches that of the 325 MHz image and the two images have been used to derive the spectral index image shown in the top-right panel of Fig. 4. We note that the flux densities of both the 325 MHz and the 1.4 GHz images are perfectly consistent with those of the WENSS and the NVSS data. At 4.8 GHz, we were able to combine data from the B and C array. Only the core and the brightest part of the lobes are detected in this image that can however be used to derive an integrated flux density for the radio source. At 8.6 GHz, we recover a D array image in which only the core of the radio galaxy is visible.

The source B2 1610+29 has an angular size of about two arcmin and a very relaxed morphology that is completely resolved out by the A configuration of the VLA at 1.4 GHz. Thus, we opted to combine only data for the B and C arrays at this frequency, obtaining a final resolution of $5\farcs5 \times 5\farcs5$ and a rms noise level of 70 μJy/beam. This is the highest resolution image we present for this source as iso-contours in the top-left panel of Fig. 5. The flux density of our B+C image is consistent, within the errors, with the NVSS flux. Therefore, we are confident to have recovered most of the flux density from the extended source structure. We also produced images at 1.4 and 4.7 GHz in the C and D configurations, respectively. These images, which have been restored with the same resolution of $17'' \times 17''$ and corrected for the primary beam attenuation, are characterized by roughly the same uv-coverage and have been used to produce the spectral index image shown in the top-right panel of Fig. 5. Finally, for the purposes of the analysis of the source integrated spectrum, we reduced separately the two IFs of the L band observation obtaining a measure of the source flux densities at 1452 and 1502 MHz.

Table 2. VLA observations summary.

Source	Array	Frequency (GHz)	Date	Duration (hours)
WNB1734+6407	A	1.4	21-Apr.-2002	5.2
	B	1.4	17-Jul.-2002	2.7
	C	1.4	20-Dec.-2002	2.4
	C	4.8	21-Dec.-2002	6.2
	D	4.8	07-Dec.-2001	3.0
WNB1829+6911	A	1.4	11-Apr.-2002	2.6
	B	1.4	17-Jul.-2002	2.7
	C	1.4	20-Dec.-2002	2.4
	C	4.8	21-Dec.-2002	0.4
	D	4.8	07-Dec.-2001	3.1
WNB1851+5707	A	1.4	26-Mar.-2002	3.0
	B	1.4	17-Jul.-2002	0.8
	C	1.4	22-Jun.-2002	2.8
	C	4.8	15-Dec.-2002	4.0
	D	4.8	08-Dec.-2001	3.2

3.3. Comments on individual sources

The VLA integrated flux density and spectral index for the individual source components are listed in Table 4.

3.3.1. WNB 1734+6407

Characterized by two relaxed lobes lacking hot-spots, the radio morphology of WNB1734+6407 resembles that of B2 0924+30, which is considered the prototype of fossil radio galaxies (Cordey 1987; but also see Jamrozy et al. 2004, for more recent

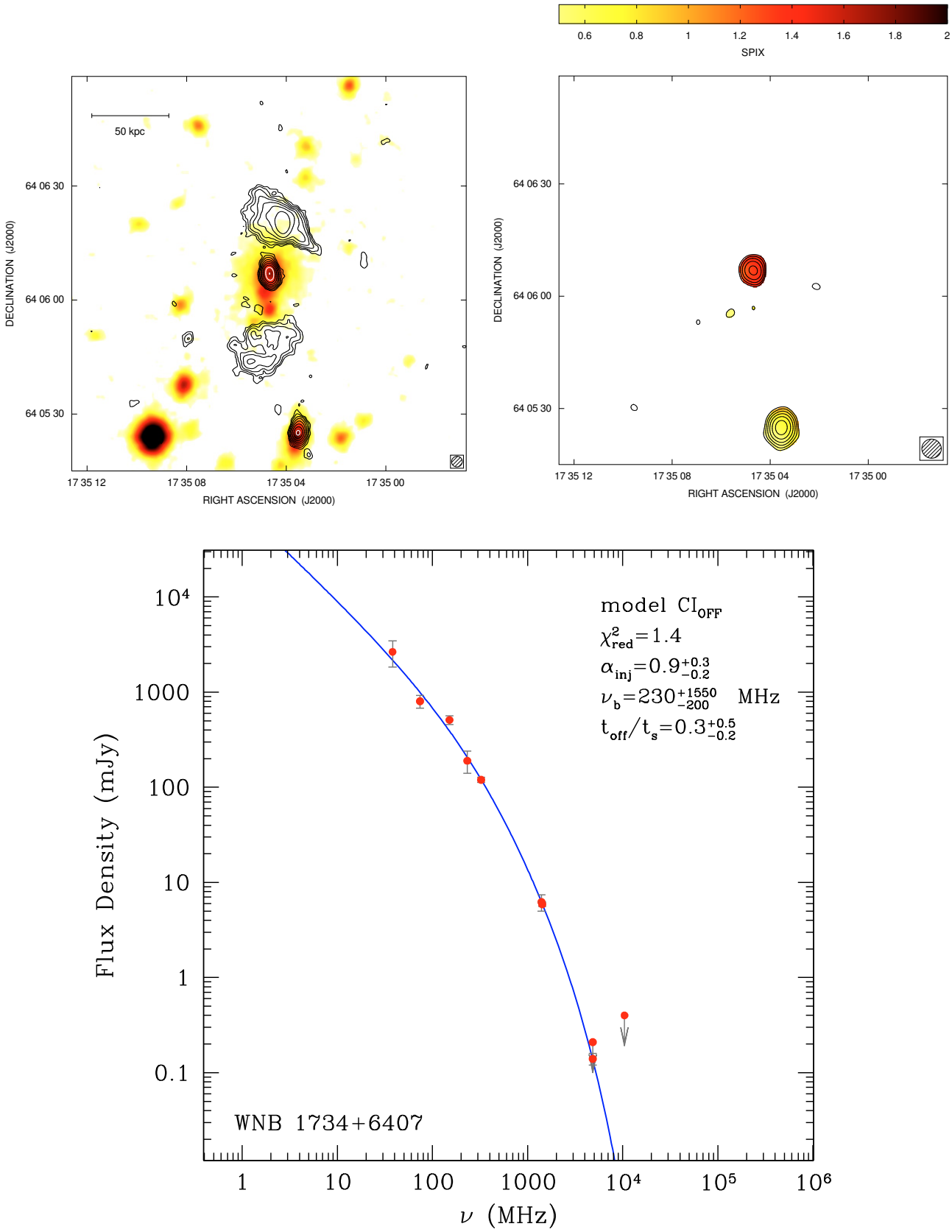

Fig. 1. WNB 1734+6407. *Top-left panel* image has been taken at 1.4 GHz with the VLA in A+B+C configuration, the restoring beam *FWHM* is $2.9'' \times 2.8''$. The contours of the radio intensity are overlaid on the optical DSS2 image. *The top-right panel* show the overlay of the spectral index image between 1.4 and 4.8 GHz with the 4.8 GHz contour levels of the VLA C+D array image. The restoring beam *FWHM* is $5.2'' \times 5.1''$. Both the 1.4 and 4.8 GHz images have the same sensitivity level of 10 μJy/beam. Radio contours start from a level of 3σ-rms and scale by $\sqrt{2}$. In the *bottom panel*, we show the integrated spectrum of the source along with the best-fit synchrotron model.

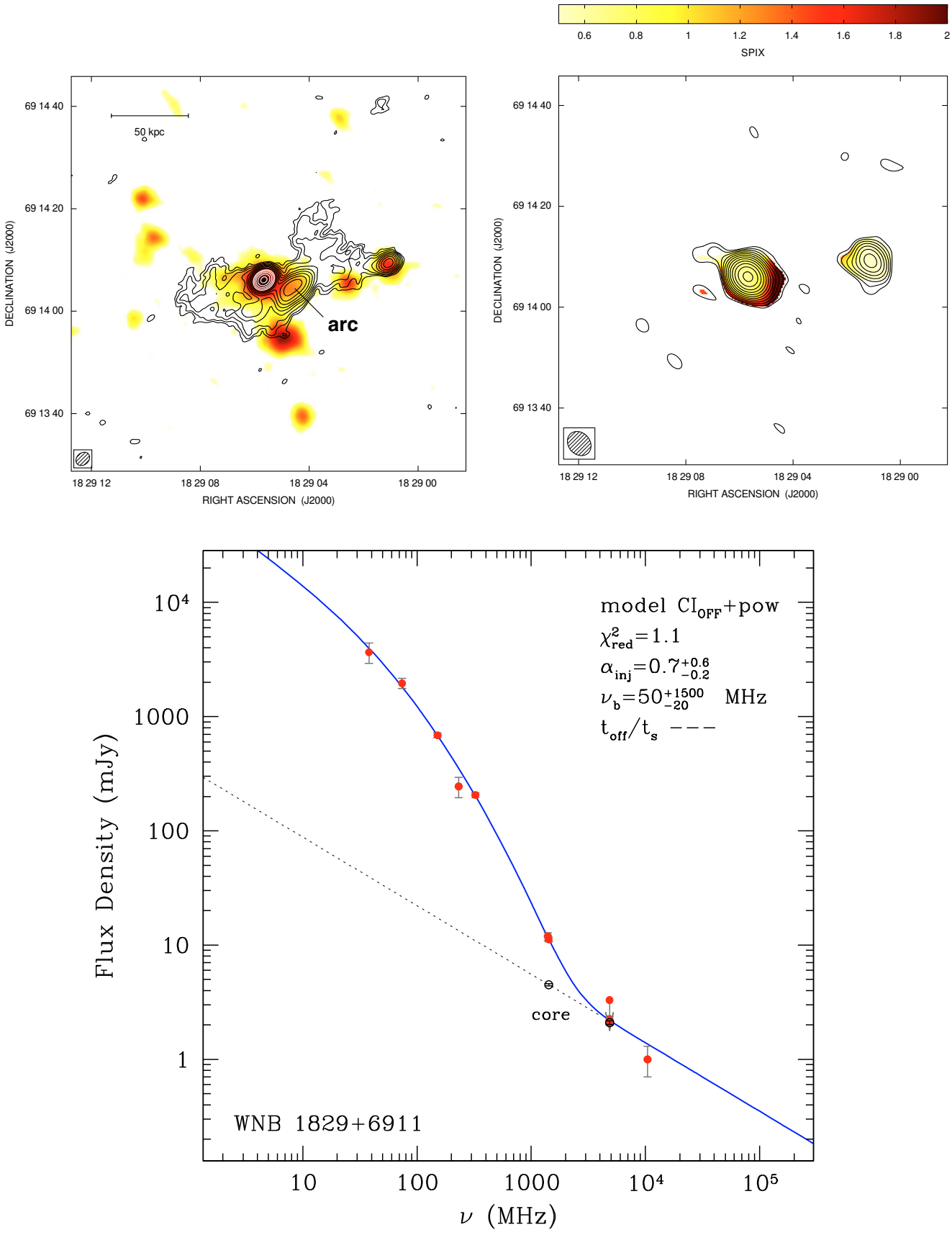

Fig. 2. WNB 1829+6911. *Top-left panel* image has been taken at 1.4 GHz with the VLA in A+B+C configuration, the restoring beam *FWHM* is 2.9″ × 2.3″. The contours of the radio intensity are overlaid on the optical DSS2 image. *The top-right panel* show the overlay of the spectral index image between 1.4 and 4.8 GHz with the 4.8 GHz contour levels of the VLA C+D array image. The restoring beam *FWHM* is 5.2″ × 4.3″. Both the 1.4 and 4.8 GHz images have the same sensitivity level of 13 μJy/beam. Radio contours start from a level of 3σ-rms and scale by $\sqrt{2}$. In the *bottom panel*, we show the integrated spectrum of the source along with the best-fit synchrotron model.

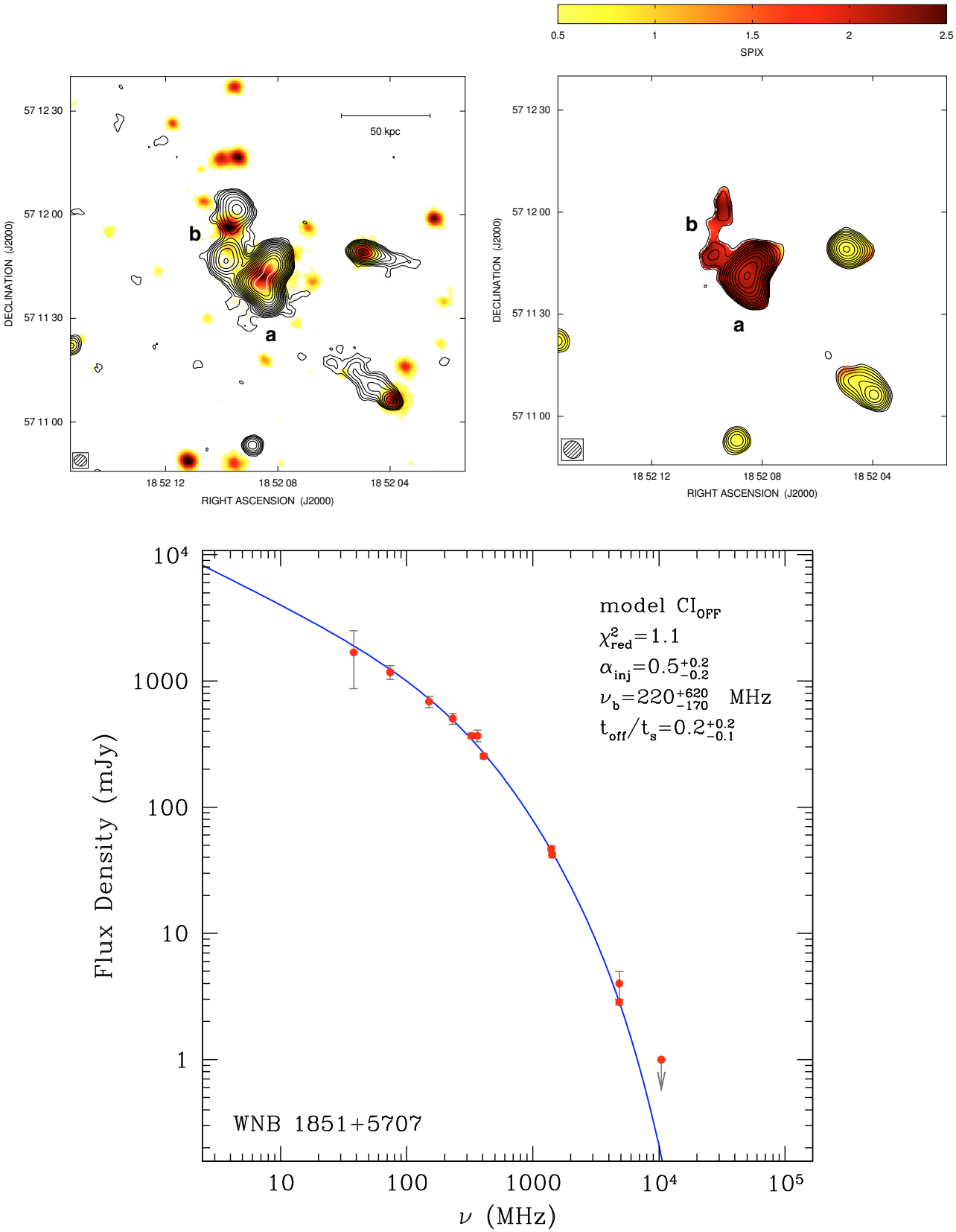

Fig. 3. WNB 1851+5707. *Top-left panel* image has been taken at 1.4 GHz with the VLA in A+B+C configuration, the restoring beam *FWHM* is $3.7'' \times 3.3''$. The contours of the radio intensity are overlaid on the optical DSS2 image. WNB 1851+5707 is composed of two distinct dying sources labeled *a* and *b*. *The top-right panel* shows the overlay of the spectral index image between 1.4 and 4.8 GHz with the 4.8 GHz contour levels of the VLA C+D array image. The restoring beam *FWHM* is $5.3'' \times 5.0''$. The sensitivity levels of the 1.4 and 4.8 GHz images are 17 and 9 μJy/beam, respectively. Radio contours start from a level of 3σ-rms and scale by $\sqrt{2}$. In *the bottom panel*, we show the integrated spectrum of the source along with the best-fit synchrotron model. The radio spectrum is representative of WNB 1851+5707a, the brighter of the two dying sources (see text).

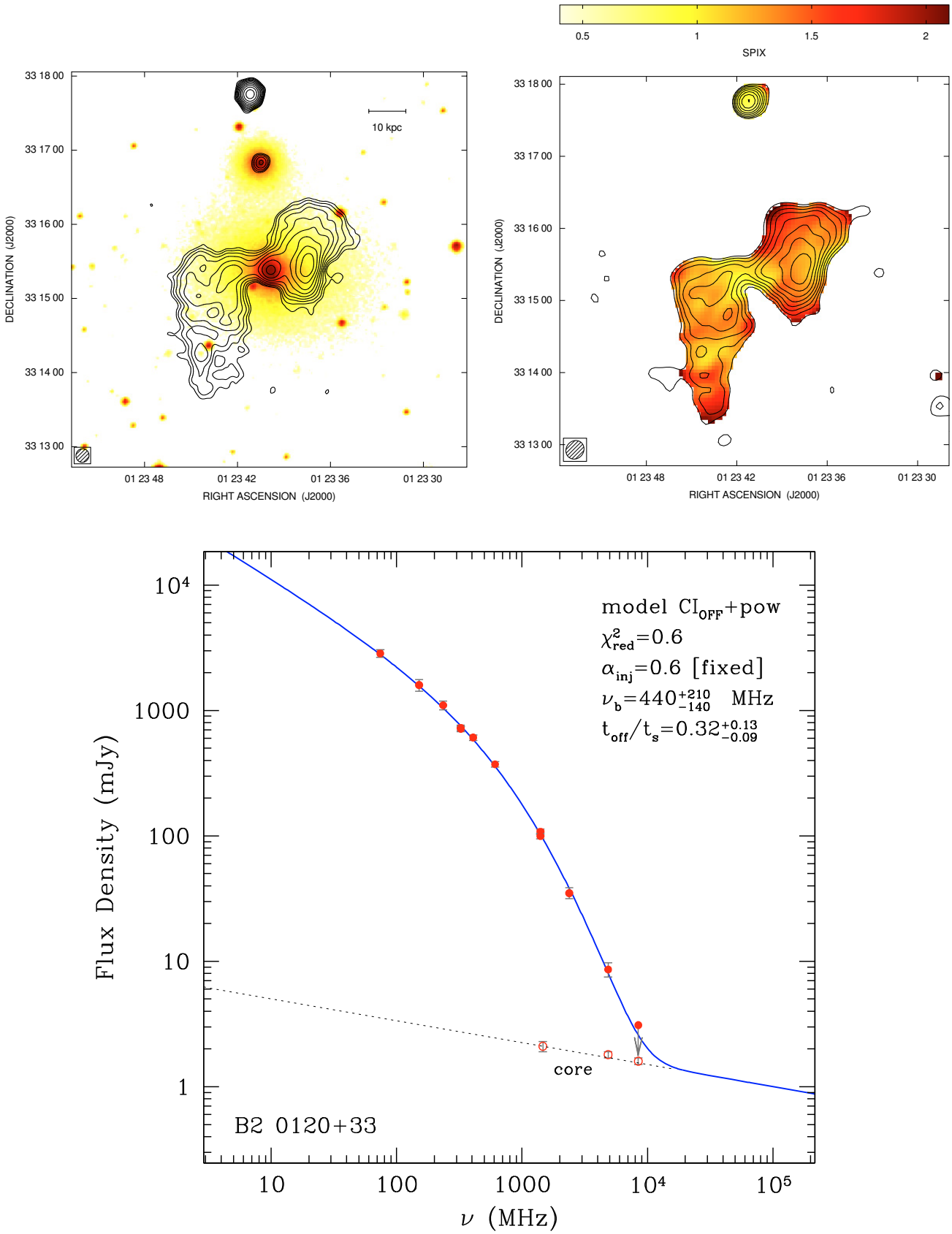

Fig. 4. B2 0120+33. *Top-left panel* image has been taken at 1.4 GHz with the VLA in B+C configuration, the restoring beam *FWHM* is 11.2″ × 10.4″. The contours of the radio intensity are overlaid on the optical DSS2 image. *The top-right panel* shows the overlay of the spectral index image between 324 MHz and 1.4 GHz with the 1.4 GHz contour levels of the VLA C array image. The restoring beam *FWHM* is 16″ × 14.5″. The sensitivity levels of 324 MHz and 1.4 GHz images are 1.4 mJy/beam and 90 μJy/beam, respectively. Radio contours start from a level of 3σ-rms and scale by $\sqrt{2}$. In *the bottom panel*, we show the integrated spectrum of the source along with the best-fit synchrotron model.

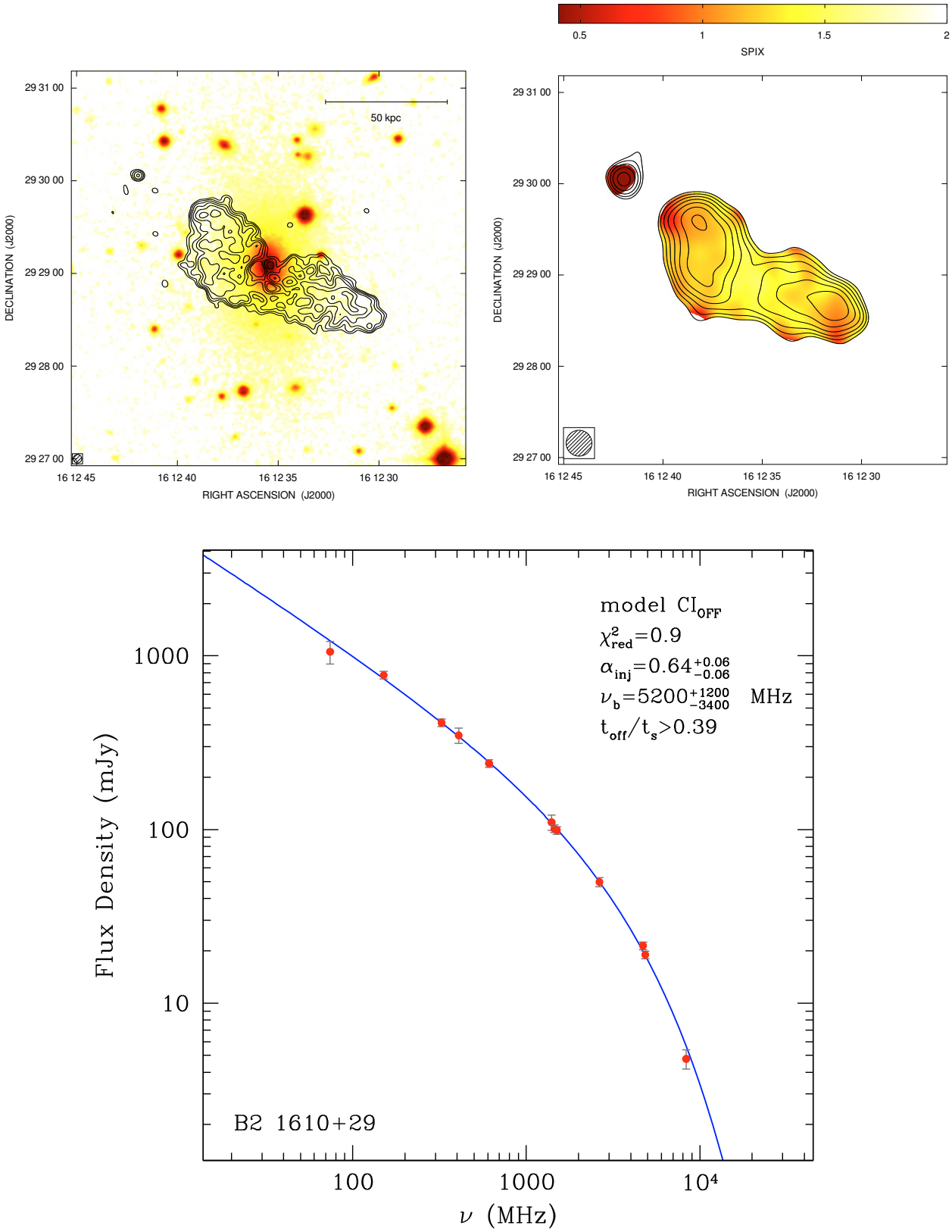

Fig. 5. B2 1610+29. *Top-left panel* image has been taken at 1.4 GHz with the VLA in B+C configuration, the restoring beam *FWHM* is 5.5″ × 5.5″. The contours of the radio intensity are overlaid on the optical DSS2 image. *The top-right panel* show the overlay of the spectral index image between 1.4 and 4.7 GHz with the 4.7 GHz contour levels of the VLA D array image. The restoring beam *FWHM* is 17″ × 17″. The sensitivity levels of the 1.4 and 4.7 GHz images are 210 and 80 μJy/beam, respectively. Radio contours start from a level of 3σ-rms and scale by $\sqrt{2}$. In *the bottom panel*, we show the integrated spectrum of the source along with the best-fit synchrotron model.

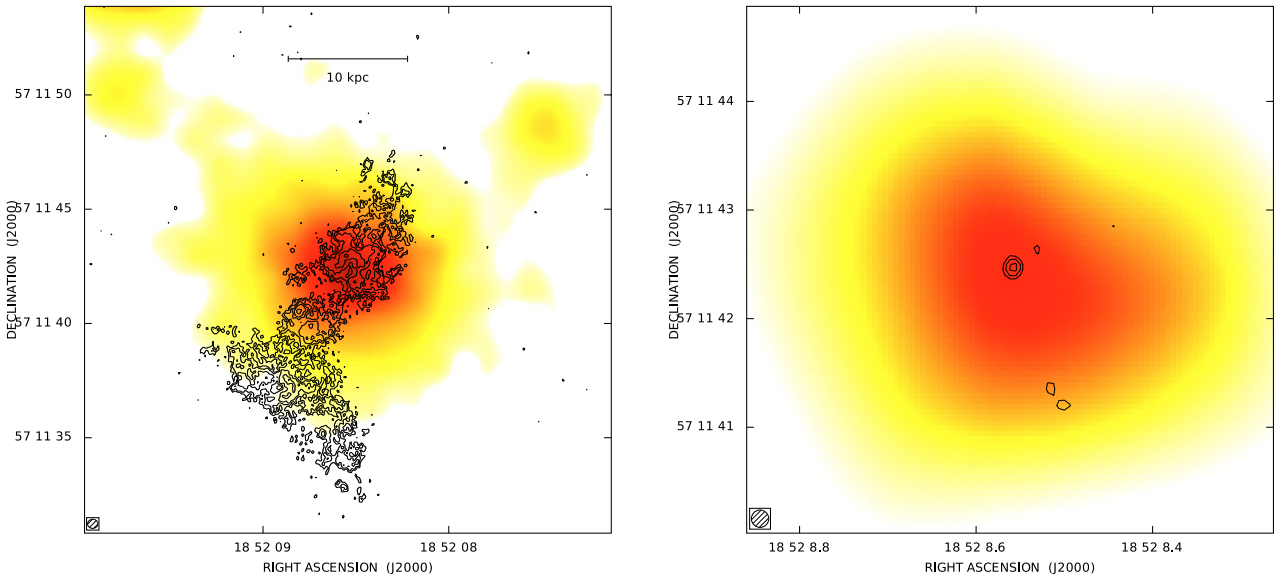

Fig. 6. MERLIN images WNB 1851+5707a at 1.4 GHz. *Left*, MERLIN+VLA radio contours at 0.″4 resolution overlaid on the DSS2 image. Contours start at 0.1 mJy/beam and increase in factors of $\sqrt{2}$. *Right*, zoom of the galaxy core. The MERLIN contours at 0.″16 resolution are overlaid to the optical DSS2 image. Contours start at 0.012 mJy/beam and increase in factors of $\sqrt{2}$. WNB 1851+5707b is not visible in the field of view of the MERLIN observation.

Table 3. Image parameter summary.

Source	Array	ν (GHz)	Beam (arcsec)	σ (μJy/beam)
WNB1734+6407	A+B+C	1.4	2.9×2.8	10
	C+D	4.8	5.2×5.1	10
WNB1829+6911	A+B+C	1.4	2.9×2.3	13
	C+D	4.8	5.2×4.3	13
WNB1851+5707	A+B+C	1.4	3.7×3.3	17
	C+D	4.8	5.3×5.0	9
B2 0120+33	B	0.324	16.0×14.5	1400
	C	1.4	13.4×12.5	50
	B+C	1.4	11.2×10.4	80
	B+C	4.8	4.0×4.0	30
	D	8.4	8.3×5.1	70
B2 1610+296	B+C	1.4	5.5×5.5	70
	C	1.4	17.0×17.0	210
	D	4.7	17.0×17.0	80

data on this source). The radio spectrum of the fossil lobes of WNB 1734+6407 is so steep that their surface brightness at 6 cm is below the sensitivity level of our observations. Thus, we can only place lower limits on the spectral index of $\alpha > 2.7$ and $\alpha > 2.3$ for the northern and southern lobe, respectively. We also observe a slightly extended component that is coincident with the galaxy center. This feature also has a quite steep spectral index, $\alpha = 1.3$, and its nature remains unclear. In the VLA A-array image (not shown), this feature is elongated in the N-S direction with an extent of about 7 kpc $\times$ 14 kpc, resembling a core-jet morphology.

3.3.2. WNB 1829+6911

The radio appearance of WNB1829+6911 is virtually identical to that of 3C 338, a nearby radio source associated with the central dominant galaxy in the cooling flow cluster Abell 2199 (Jones & Preston 2001). In both sources, we observe fossil plasma remaining from a previous activity in conjunction with a restarting core. The extended emission of WNB1829+6911 has very steep spectra with $\alpha > 1.6$ and $\alpha > 1.9$, respectively, for the W and E-lobe. The source exhibits a bright core with a much flatter spectrum, $\alpha = 0.6$. This region of the radio source is most probably powered by a new couple of restarting jets. The core emission is responsible for the high-frequency flattening seen in the source integrated spectrum (Fig. 2 bottom panel). An arc-like feature with a very steep spectrum ($\alpha > 2.5$) can be seen on the SW side of the core (Fig. 2 top-left panel).

3.3.3. WNB 1851+5707

Our VLA images reveal that WNB1851+5707 is in reality composed by two distinct dying radio galaxies. For source WNB1851+5707a, we measured a spectral index $\alpha = 2.2$ while for WNB1851+5707b we measure $\alpha = 2.3$. This association is intriguing because of the rarity of this kind of sources. According to the interpretation that these are relic sources, we found that, at the sensitivity limits of our VLA observations, they possess neither radio jets on kpc scale nor bright hot spots inside the fossil lobes. The two hosting galaxy have nearly the same redshifts (see Table 1), making the possibility of a spatial casual coincidence even more unlikely.

We note that WNB1851+5707 is located at the center of a galaxy cluster, see Sect. 6. Thus, it could be that the two dying lobes of WNB1851+5707b are indeed two previous outbursts of WNB1851+5707a that are emerging from the cluster center because of the buoyancy forces. However, this scenario seems unlikely because of the almost perfect spatial coincidence of WNB1851+5707b with the second galaxy.

3.3.4. B2 0120+33

The radio source is asymmetric, the west lobe being brighter and smaller that the east one. The radio emission is very weak and diffuse. A similar morphology has been observed in GMRT images at 235 and 610 MHz by Giacintucci et al. (2010, in prep.). At arcsecond resolution, the only compact structure is the faint unresolved core. There is no evidence of kpc-scale jets in any

Table 4. VLA integrated flux densities and spectral indexes of sources components.

Source	Component	Size kpc × kpc	$S_{1.4}$ mJy	$S_{4.8}$ mJy	$\alpha_{1.4}^{4.8}$
WNB1734+6407	N-Lobe	63 × 42	2.9 ± 0.03	<0.1	>2.7
	S-Lobe	60 × 42	1.7 ± 0.03	<0.1	>2.3
	Core-Jet?	14 × 7	0.7 ± 0.01	0.14 ± 0.02	1.3 ± 0.1
	Total	120 × 62	5.9 ± 0.1	0.14 ± 0.02	3.0 ± 0.1
WNB1829+6911	E-Lobe	72 × 47	2.1 ± 0.07	<0.2	>1.9
	W-Lobe	69 × 41	1.4 ± 0.06	<0.2	>1.6
	Arc	33 × 16	2.1 ± 0.05	<0.1	>2.5
	Core	–	4.5 ± 0.02	2.1 ± 0.03	0.62 ± 0.01
	Total	135 × 61	11.2 ± 0.1	2.1 ± 0.03	1.4 ± 0.01
WNB1851+5707a	Total	15 × 30	41.8 ± 0.08	2.8 ± 0.04	2.2 ± 0.1
WNB1851+5707b	N-Lobe	23 × 17	2.6 ± 0.07	0.17 ± 0.02	2.2 ± 0.3
	S-Lobe	19 × 19	2.3 ± 0.05	0.13 ± 0.02	2.3 ± 0.3
	Total	50 × 25	4.9 ± 0.06	0.3 ± 0.03	2.3 ± 0.2
B2 0120+33	E-Lobe	47 × 24	43.6 ± 0.3	3.64 ± 0.6	2.0 ± 0.14
	W-Lobe	32 × 22	56.5 ± 0.2	4.5 ± 0.5	2.1 ± 0.1
	Core	–	2.1 ± 0.2	1.8 ± 0.1	0.13 ± 0.09
	Total	73 × 40	99.5 ± 1.5	8.6 ± 1.1	2.0 ± 0.1
B2 1610+29	Total	100 × 30	100 ± 1.4	15.5 ± 0.3	1.5 ± 0.02

of our images. Hence, the extended lobes of B2 0120+33 were produced by an earlier phase of activity.

3.3.5. B2 1610+29

The morphology of B2 1610+29 is exactly the one we would expect for a dying radio source: two symmetric and relaxed radio lobes sit on the opposite side of the host galaxy, there are neither jets nor hot-spots in the lobes, and the host galaxy lacks a bright radio core. All these features are strong indications that B2 1610+29 is a dying source where only the fading lobes are still visible. The source has an overall linear size of about 100 kpc with a small offset of the source major axis to south-east with respect to the position of the galaxy. The host galaxy of B2 1610+29 was studied with the VLBA at 5 GHz by Liuzzo et al. (2010). They did not detect any compact radio structure in their high resolution images. These results also suggest that B2 1610+29 is most likely a dying radio source.

4. MERLIN observations and data reduction

Among the five dying sources, WNB1851+5707a is the most compact and bright. We observed this source with the MERLIN interferometer to unveil the possible presence of a core or jets unresolved by the VLA images. WNB1851+5707a was observed in three days on April 2005 for a total on-source time of about 18 h with MERLIN (6 antennas) and Lovell. The observing frequency was 1.408 GHz, with a bandwidth of 16 MHz in both circular polarizations; the data were taken in spectral-line mode (32 × 0.5–MHz channels). OQ208 (1.00 Jy) and 3C 286 (14.79 Jy) were used as flux calibration sources, while 1851+609 (0.25 Jy) was used as a phase calibrator. The 1.4 GHz data from MERLIN and the VLA A-array were combined to increase the brightness sensitivity and uv-coverage, to image finer details of the components seen in the L-Band MERLIN images, whilst also imaging the more diffuse radio emission observed in the VLA images. The length of the shortest baseline of the MERLIN array at 1.4 GHz is 6 km. At this frequency, the interferometer is then insensitive to structures larger than $\vartheta_{\rm max}^{1.6\ {\rm GHz}} = 4''$ (8.5 kpc at the distance of WNB1851+5707a). The combination of the 1.4 GHz MERLIN data with the VLA A-array data gives a shortest baseline of 0.68 km, so that $\vartheta_{\rm max}^{1.4{\rm GHz}} = 64''$ (136 kpc). Several images were produced using the AIPS task IMAGR, and deconvolved with the multi-scale CLEAN algorithm. The full-resolution 0.″16 MERLIN image is shown in the right panel of Fig. 6. The only detected feature is a faint point-like source with a flux density of 0.4 ± 0.1 mJy at the center of the optical galaxy. There is no evidence of active radio jets. Most of the flux density of WNB1851+5707a indeed comes from the extended structure already mapped in the VLA observations, confirming that WNB1851+5707a is a "de-energized" radio source. The MERLIN image is presented in combination with the VLA A-array at a resolution of 0.″4 in the left panel of Fig. 6. The MERLIN+VLA contours reveal that WNB1851+5707a is an amorphous radio source with a linear size of roughly 30 kpc × 15 kpc. The radio source is also considerably asymmetric being far more extended to the south of the optical galaxy.

5. Analysis of the radio source spectra

5.1. Compilation of integrated spectra

In addition to our own observations, we collected all the spectral information available in the literature for the five dying radio galaxies. We used the CATS (the on-line Astrophysical CATalogs support System[4]; Verkhodanov et al. 1997) to recover data from catalogs at different frequencies. We placed all the flux densities from all these references onto the absolute flux density of Baars et al. (1977) by scaling for the multiplicative factor listed in Helmboldt et al. (2008). The resulting catalogued flux densities ($S_\nu^{\rm catalogued}$) are given in Col. 3 of Table 5. The various catalogs we used to compile the integrated spectra have quite different angular resolutions. It is therefore necessary to remove the flux density due to confusing sources to recover a reliable spectrum for each dying source. We estimated the contribution of the confusing sources at each frequency on the basis of the

[4] http://cats.sao.ru/

Table 5. Integrated spectra.

Source	Frequency MHz	$S_\nu^{\rm catalogued}$ mJy	$f_{\rm Baars}$	Reference	$S_\nu^{\rm confusion}$ mJy	S_ν mJy
WNB 1734+6407	38	2699 ± 818	0.818	8C, Hales et al. (1995)	50 ± 12	2649 ± 818
	74	810 ± 120	1.0	VLSS, Cohen et al. (2007)	8 ± 3	802 ± 120
	151	524 ± 52	0.904	6CIII, Hales et al. (1990)	14 ± 2	510 ± 52
	232	200 ± 50	1.0	MIYUN, Zhang et al. (1997)	9.8 ± 1.1	190 ± 50
	325	123 ± 7.3	1.0	WENSS, Rengelink et al. (1997)	2.8 ± 0.5	120 ± 7
	1400	7.2 ± 1.2	1.0	NVSS, Condon et al. (1998)	1.04 ± 0.04	6.2 ± 1.2
	1425	5.9 ± 0.1	1.0	Effelsberg 100-m, this work	–	5.9 ± 0.1
	4850	0.2 ± 0.02	1.0	VLA, this work	0.63 ± 0.07	<0.21
	4850	0.14 ± 0.02	1.0	Effelsberg 100-m, this work	–	0.14 ± 0.02
	10 450	<0.4	1.0	VLA, this work	–	<0.4
WNB 1829+6911	38	3681 ± 740	0.818	8C, Hales et al. (1995)	21 ± 27	3661 ± 740
	74	1960 ± 200	1.0	VLSS, Cohen et al. (2007)	2.0 ± 0.76	1958 ± 200
	151	694 ± 31	0.904	6CIV, Hales et al. (1991)	7.2 ± 4.9	687 ± 31
	232	250 ± 50	1.0	MIYUN, Zhang et al. (1997)	5.2 ± 2.7	245 ± 50
	325	207 ± 9	1.0	WENSS, Rengelink et al. (1997)	1.2 ± 0.22	209 ± 9
	1400	12.6 ± 0.9	1.0	NVSS, Condon et al. (1998)	0.71 ± 0.02	11.9 ± 0.9
	1425	11.2 ± 0.1	1.0	VLA, this work	–	11.2 ± 0.1
	4850	2.25 ± 0.12	1.0	CATS, Verkhodanov et al. (1997)	–	2.25 ± 0.12
	4850	<3.3	1.0	Effelsberg 100-m, this work	–	<3.3
	4860	2.1 ± 0.03	1.0	VLA, this work	–	2.1 ± 0.03
	10 450	1.3 ± 0.3	1.0	Effelsberg 100-m, this work	0.35 ± 0.09	1.0 ± 0.3
WNB 1851+5707	38	1800 ± 818	0.818	8C, Hales et al. (1995)	114 ± 11.9	1686 ± 818
	74	1240 ± 150	1.0	VLSS, Cohen et al. (2007)	65.7 ± 5.7	1174 ± 150
	151	723 ± 72	0.904	6CV, Hales et al. (1993)	36.3 ± 2.4	687 ± 72
	232	530 ± 50	1.0	MIYUN, Zhang et al. (1997)	25.5 ± 1.4	505 ± 50
	325	387 ± 4.4	1.0	WENSS, Rengelink et al. (1997)	19.3 ± 0.9	368 ± 5
	365	437 ± 41	1.041	TEXAS, Douglas et al. (1996)	51.8 ± 1.8	385 ± 41
	408	270 ± 10	1.091	B3.3, Altieri et al. (1999)	16.0 ± 0.7	254 ± 10
	1400	53 ± 2.3	1.0	NVSS, Condon et al. (1998)	5.78 ± 0.12	47 ± 2.3
	1425	41.9 ± 0.1	1.0	VLA, this work	–	41.9 ± 0.1
	4850	6.1 ± 1.0	1.0	Effelsberg 100-m, this work	2.09 ± 0.09	4.0 ± 1.0
	4850	2.85 ± 0.03	1.0	VLA, this work	–	2.85 ± 0.03
	10 450	1.2 ± 0.3	1.0	Effelsberg 100-m, this work	1.12 ± 0.08	<1.0
B2 0120+33	74	2847 ± 200	1.0	VLSS image, this work	–	2847 ± 200
	151	1690 ± 170	0.904	6CVI, Hales et al. (1993)	96.3 ± 3.6	1594 ± 170
	235	1100 ± 88	1.0	GMRT, Giacintucci et al., in prep.	–	1100 ± 88
	324	727 ± 11.7	1.0	VLA, this work	–	727 ± 11.7
	325	715 ± 16	1.0	WENSS image, this work	–	715 ± 16
	408	660 ± 20	1.0	Feretti & Giovannini (1980)	50.5 ± 2.5	609 ± 20
	610	372 ± 18.6	1.0	GMRT, Giacintucci et al., in prep.	–	372 ± 18.6
	1400	108 ± 0.5	1.0	NVSS image, this work	–	108 ± 0.5
	1400	99.5 ± 1.5	1.0	VLA, this work	–	99.5 ± 1.5
	2380	35 ± 3.5	1.0	ARECIBO, Dressel & Condon (1978)	–	35.0 ± 3.5
	4860	8.6 ± 1.1	1.0	VLA, this work	–	8.6 ± 1.1
	8460	<3.1	1.0	VLA, this work	–	<3.1
B2 1610+29	74	1055 ± 157	1.0	VLSS image, this work	–	1055 ± 157
	151	774 ± 9.5	1.237	7C, Riley et al. (1989)	–	774 ± 9.5
	325	412 ± 5.2	1.0	WENSS, Rengelink et al. (1997)	–	412 ± 5.2
	408	349 ± 35	1.091	B2, Colla et al. (1970)	–	349 ± 35
	610	240 ± 12	1.0	GMRT, Giacintucci et al. (2007)	–	240 ± 12
	1400	110 ± 11	1.0	NVSS image, this work	–	110 ± 11
	1452	101 ± 2	1.0	VLA, this work	–	101 ± 2
	1502	98.8 ± 2	1.0	VLA, this work	–	98.8 ± 2
	2639	49.8 ± 3	1.0	Effelsberg 100-m, this work	–	49.8 ± 3
	4710	21.4 ± 0.3	1.0	VLA, this work	–	21.4 ± 0.3
	4850	19.0 ± 0.4	1.0	Effelsberg 100-m, this work	–	19.0 ± 0.4
	8350	4.8 ± 0.6	1.0	Effelsberg 100-m, this work	–	4.8 ± 0.6

Table 6. Physical parameters of the dying sources. Uncertainties on fit parameters are at 1-σ level.

Source	$\alpha_{\rm inj}$	$\nu_{\rm b}$ MHz	$t_{\rm OFF}/t_{\rm s}$	L_{151} W/Hz	$B_{\rm min}$ μG	$u_{\rm min}$ erg/cm^3	$t_{\rm s}$ Myr	$t_{\rm CI}$ Myr	$t_{\rm OFF}$ Myr
WNB1734+6407	$0.9^{+0.3}_{-0.2}$	230^{+1550}_{-200}	$0.3^{+0.5}_{-0.2}$	2.6×10^{25}	10	8.3×10^{-12}	86	60	26
WNB1829+6911	$0.7^{+0.6}_{-0.2}$	50^{+1500}_{-20}	–	7.6×10^{25}	7.8	5.3×10^{-12}	218	–	–
WNB1851+5707a	$0.5^{+0.2}_{-0.2}$	220^{+620}_{-170}	$0.2^{+0.2}_{-0.1}$	1.8×10^{25}	9.8	8.9×10^{-12}	90	72	18
B2 0120+33 Global spec.	0.6 (fixed)	440^{+210}_{-140}	$0.3^{+0.1}_{-0.1}$	1×10^{24}	5.2	2.4×10^{-12}	141	99	42
Sp. index profile	0.65 (fixed)	1840^{+480}_{-380}	>0.8				69	<13	>55
B2 1610+29 Global spec.	$0.64^{+0.06}_{-0.06}$	5200^{+1200}_{-3400}	>0.39	1.4×10^{24}	3.2	9.3×10^{-13}	55	<33	>22
Sp. index profile	0.6 (fixed)	4770^{+600}_{-500}	$0.8^{+0.1}_{-0.1}$				58	12	46

VLA images at 1.4 GHz and 4.8 GHz. The confusion flux density at a given frequency is given by the sum

$$S_\nu^{\rm confusion} = \sum_{i=1}^{N_\nu} S^i_{1425}(\nu/1425)^{-\alpha_i}, \quad (2)$$

where ν is the frequency in MHz, S_{1425} is the flux density measured in the VLA image at 1425 MHz, α_i is the spectral index of the confusing source measured from the VLA images at 1.4 and 4.8 GHz, and N_ν is the number of sources that fall within the beam of the catalog at frequency ν. Finally, we calculated the source flux density at a given frequency as

$$S_\nu = S_\nu^{\rm catalogued} - S_\nu^{\rm confusion}, \quad (3)$$

which is the quantity listed in Col. 7 of Table 5.

The total spectra of the five dying radio sources are show in the bottom panels of Figs. 1 to 5. For four of them, namely WNB1734+6407, WNB1851+5707, B2 0120+33, and B2 1610+29, the integrated spectrum has a strong exponential cutoff in the observed frequency range. However, for WNB 1829+6911 there is a clear flattening of the integrated spectrum at high frequency. This flattening is due to the core-jet component that dominates the spectrum at the highest frequencies.

5.2. Spectral modeling of the integrated spectra

We modeled the integrated spectra assuming the radiative energy losses to be dominant with respect to other processes (e.g. adiabatic losses). The pitch angles of the radiating electrons are assumed to be continually isotropized in a time that is shorter than the radiative timescale. According to this assumption, the synchrotron energy losses are statistically the same for all electrons. After its birth, the source is supposed to be fuelled at a constant rate (i.e. *the continuous injection phase*) by the nuclear activity, for a duration $t_{\rm CI}$. The injected particles are assumed to have a power-law energy spectrum $N(\epsilon) \propto \epsilon^{-\delta_{\rm inj}}$, which will result in a power law radiation spectrum with spectral index $\alpha_{\rm inj} = (\delta_{\rm inj} - 1)/2$. In this phase, the source radio spectrum changes as a function of time in a way described by the shift of break frequency $\nu_{\rm b}$ to ever lower values as the time, t_s, increases

$$\nu_{\rm b} \propto \frac{B}{(B^2 + B^2_{\rm IC})^2 t_{\rm s}^2}, \quad (4)$$

where B and $B_{IC} = 3.25(1+z)^2$ are the source magnetic field and the inverse Compton equivalent magnetic field, respectively. Below and above $\nu_{\rm b}$, the spectral indices are respectively $\alpha_{\rm inj}$ and $\alpha_{\rm inj} + 0.5$.

At the time $t_{\rm CI}$, the power supply from the nucleus is switched-off. After that a new phase of duration $t_{\rm OFF}$ begins (i.e. the *dying phase*). A new break frequency $\nu_{\rm b\,high}$ then appears, beyond which the radiation spectrum drops exponentially. This second high frequency break is related to the first by

$$\nu_{\rm b\,high} = \nu_{\rm b}\left(\frac{t_{\rm s}}{t_{\rm OFF}}\right)^2, \quad (5)$$

where $t_{\rm s} = t_{\rm CI} + t_{\rm OFF}$ is the total source age (see e.g. Komissarov & Gubanov 1994; Slee et al. 2001; Parma et al. 2007).

Thus, the above synchrotron model (hereafter CI$_{\rm OFF}$) is described by four parameters

i) $\alpha_{\rm inj}$, the injection spectral index;
ii) $\nu_{\rm b}$, the lowest break frequency;
iii) $t_{\rm OFF}/t_{\rm s}$, the dying to total source age ratio;
iv) *norm*, the flux normalization.

In the CI$_{\rm OFF}$ model the magnetic field strength is assumed to be uniform within the source.

The fit to the CI$_{\rm OFF}$ is shown as a line in the bottom panels of Figs. 1 to 5, while the best-fit parameters are listed in Table 6. The fits are very good for all the five dying sources discussed below:

- in the case of WNB1734+6407, the overall radio spectrum is particularly steep with an exponential cut-off beyond a frequency of about 230 MHz. The spectral fit indicates that the source has spent about 30% of its total lifetime ($t_{\rm OFF}/t_{\rm s} = 0.3$) in the dying phase;
- the source WNB 1829+6911 is a different case. Its low frequency spectrum is rather steep, but strongly flattens above 1.4 GHz, because of a bright core that is clearly detected in the 4.8 GHz images. The core has a flat spectrum characterized by $\alpha = 0.6$ between these two frequencies and is probably still active. To account for this component in the spectral fit, we added a power law to the CI$_{\rm OFF}$ model, using the observed spectral index and flux density as the normalization. In this case, we may be observing fading lobes (produced by a previous duty cycle), in conjunction with restarting activity in the core. However, from the spectral fit we are unable to determine the relative duration of the dying phase since the rising of the new flat spectrum core canceled out the second high break frequency $\nu_{\rm b\,high}$ of the fossil lobes;
- both dying sources *a* and *b* contribute to the total spectrum of WNB 1851+5707. However, WNB 1851+5707a is ten times brighter than WNB 1851+5707b (see Table 4). If the radio sources have a similarly curved spectral shape, we can reasonably assume that the total spectrum of WNB 1851+5707 is representative of source *a* alone. The radio spectrum of WNB 1851+5707a is consistent with an injection spectral index of about $\alpha_{\rm inj} = 0.5$ and a cut-off that is almost exponential beyond a break frequency of 220 MHz. The duration of the dying phase is 20% of the total source age. For

WNB 1851+5707b, we do not have the possibility of measuring its complete total radio spectrum, given its closeness to its brighter companion. We can report only the particularly steep spectral index of the two fading lobes as seen in our VLA images $\alpha_{1.4}^{4.8} \simeq 2.3$;

– we fitted the integrated spectrum of B2 0120+33 with the CI_{OFF} model plus a power law that accounts for the emission of the radio core. The radio core however is very faint and its emission becomes important only at frequencies greater than 10 GHz. At lower frequencies, the source spectrum is dominated by the fading radio lobes and can be modeled with an injection spectral index of $\alpha_{inj} = 0.6$ and a break frequency of about 440 MHz. According to the spectral fit, the duration of the dying phase should be about 30% of the total source age;

– finally, the source B2 1610+29 has an injection spectral index of $\alpha_{inj} = 0.6$ and a break frequency somewhat higher with respect to the other dying source presented above, $\nu_b \simeq 5200$ MHz. Owing to the lack of spectral information at frequencies higher that 10 GHz, we can only put a lower limit on the duration of the dying phase $t_{OFF}/t_s > 0.4$. However, for this source we have a very good spatially resolved spectral-index image and we can try to get some additional constraints on the source age from the fit of the spectral index profile.

5.3. Modeling of the spectral index profile in B2 0120+33 and B2 1610+29

The two dying galaxies B2 0120+33 and B2 1610+29 are extended enough to permit a study of the spectral variation along the fading lobes.

For B2 0120+33, the profile of the spectral index between 325 MHz and 1.4 GHz can be traced along all the lobes (see Fig. 7). The spectral index trend was obtained by averaging the flux densities at the two frequencies in circular regions of 36″ in diameter centered as shown in the inset of Fig. 7. The regions are much larger than the beam so that the spectral index measurements are effectively independent. The observed spectral index trend is rather smooth with $\alpha_{0.3}^{1.4}$ close to about 1.2 over the whole radio source. Assuming a constant source expansion-velocity, the spectral index at a given distance from the core can be related to the synchrotron age of the electrons at that location. We assume that in B2 0120+33 the youngest electrons were injected by the jets close to the core during the active phase. This behavior is the typical one we observe in many FRI-type tailed radio sources (see e.g. Parma et al. 1999). In this case, we expect that the break frequency scales as

$$\nu_b(d) = \frac{\nu_b(d_{max})}{[(d/d_{max}) \cdot (1 - t_{OFF}/t_s) + t_{OFF}/t_s]^2}, \quad (6)$$

where the distance d ranges from $d = 0$ at the location of the galaxy, up to $d = d_{max}$ at the edge of each lobe. Thus, the break frequency along the lobes varies from a minimum of ν_b, at $d = d_{max}$, up to a maximum of $\nu_{b\,high}$, at $d = 0$. The two limiting break frequencies ν_b and $\nu_{b\,high}$ are exactly the same as given in Eqs. (4) and (5), respectively. In Fig. 7, we report the fit to the observed trend obtained in the case of $\alpha_{inj} = 0.65$ for different values of t_{OFF}/t_s. It is clear that low values of t_{OFF}/t_s correspond to spectral index gradients that are too steep compared to the observed one. As t_{OFF}/t_s increases, however, the expected spectral index trends get flatter and flatter and a best fit is found for $t_{OFF}/t_s \geq 0.8$.

In the case of B2 1610+29, the profile of the 1.4 to 4.8 GHz spectral index can be traced all along the lobes (see Fig. 8). The spectral index trend has been obtained by averaging the flux densities at the two frequencies in boxes perpendicular to the source major axis. The boxes are as wide as the beam so that the spectral index measurements are effectively independent. The observed spectral index trend is rather smooth with $\alpha_{1.4}^{4.8}$ ranging from about 1.2 at the edge of the lobes up to about 1.4 at the center of the radio source. In this particular case, we assume that the electrons were injected by the jets close to the end of each of the two lobes during the active phase. This spectral behavior is common in FRII type radio sources but is also found in some FRI type radio sources (see Parma et al. 1999). In this case, we expect that the break frequency scales as

$$\nu_b(d) = \frac{\nu_b(d_{max})}{\{[(d_{max} - d)/d_{max}] \cdot (1 - t_{OFF}/t_s) + t_{OFF}/t_s\}^2}, \quad (7)$$

where the distance d ranges from $d = 0$ at the location of the galaxy, up to $d = d_{max}$ at the edge of each lobe. Thus, the break frequency along the lobes varies from a minimum of ν_b, at $d = 0$, down to a maximum of $\nu_{b\,high}$, at $d = d_{max}$. In Fig. 8, we report the fit to the observed trend obtained in the case of $\alpha_{inj} = 0.6$ for different values of t_{OFF}/t_s. It is clear that low values of t_{OFF}/t_s correspond to spectral index gradients that are too steep relative to the observed one. As t_{OFF}/t_s increases, however, the expected spectral index trends get flatter and flatter and a best fit is found for $t_{OFF}/t_s = 0.8 \pm 0.1$.

The behavior of the spectral index seen in B2 0120+33 and B2 1610+29 may be typical of many dying sources. In practice, as a result of the jet switch-off, any pre-existing spectral index gradient along the lobes is rapidly erased as the break frequency reaches roughly the same value in each part of the source. We can therefore expect that extreme dying sources, i.e. those for which $t_{OFF}/t_s \simeq 1$, are characterized by very uniform spectral index distributions along the fading lobes. As the dying source gets older, the spectral index increases systematically but with small variations from point to point.

5.4. Equipartition parameters

We performed the minimum energy calculation for the five dying galaxies by considering the source power at 151 MHz, where the energy losses of the synchrotron electrons are less dramatic, and the volumes as measured from the VLA images at arcsecond resolution. In the calculation of the source power, we used the 151 MHz flux density after the deconvolution of confusing sources. The resulting monochromatic powers in the source rest-frame, L_{151}, are listed in Table 6 and place them below the FRI-FRII division (Fanaroff & Riley 1974).

We assume that the radio sources contain relativistic particles and uniformly distributed magnetic fields in energy equipartition conditions. The equipartition parameters (magnetic field B_{min} and energy density u_{min}) are generally computed assuming that the relativistic particle energies are confined between a minimum ϵ_{low} and a maximum ϵ_{high}, corresponding to the observable radio frequency range, typically 10 MHz–100 GHz (see, e.g., Pacholczyk 1970). This choice minimizes the source energetics required by the observed radiation in the radio band. However, a fixed frequency range corresponds to an energy range that depends on the source magnetic field, which may change from source to source. A fixed frequency-range computation would miss the contribution from lower energy electrons, since the ϵ_{low} corresponding to 10 MHz is higher than 200 MeV for $B_{min} \leq 30\ \mu G$ (Brunetti et al. 1997; and Beck & Krause 2005). Because of this, we have computed the equipartition parameters assuming a fixed low energy cutoff $\epsilon_{low} = 10$ MeV. The

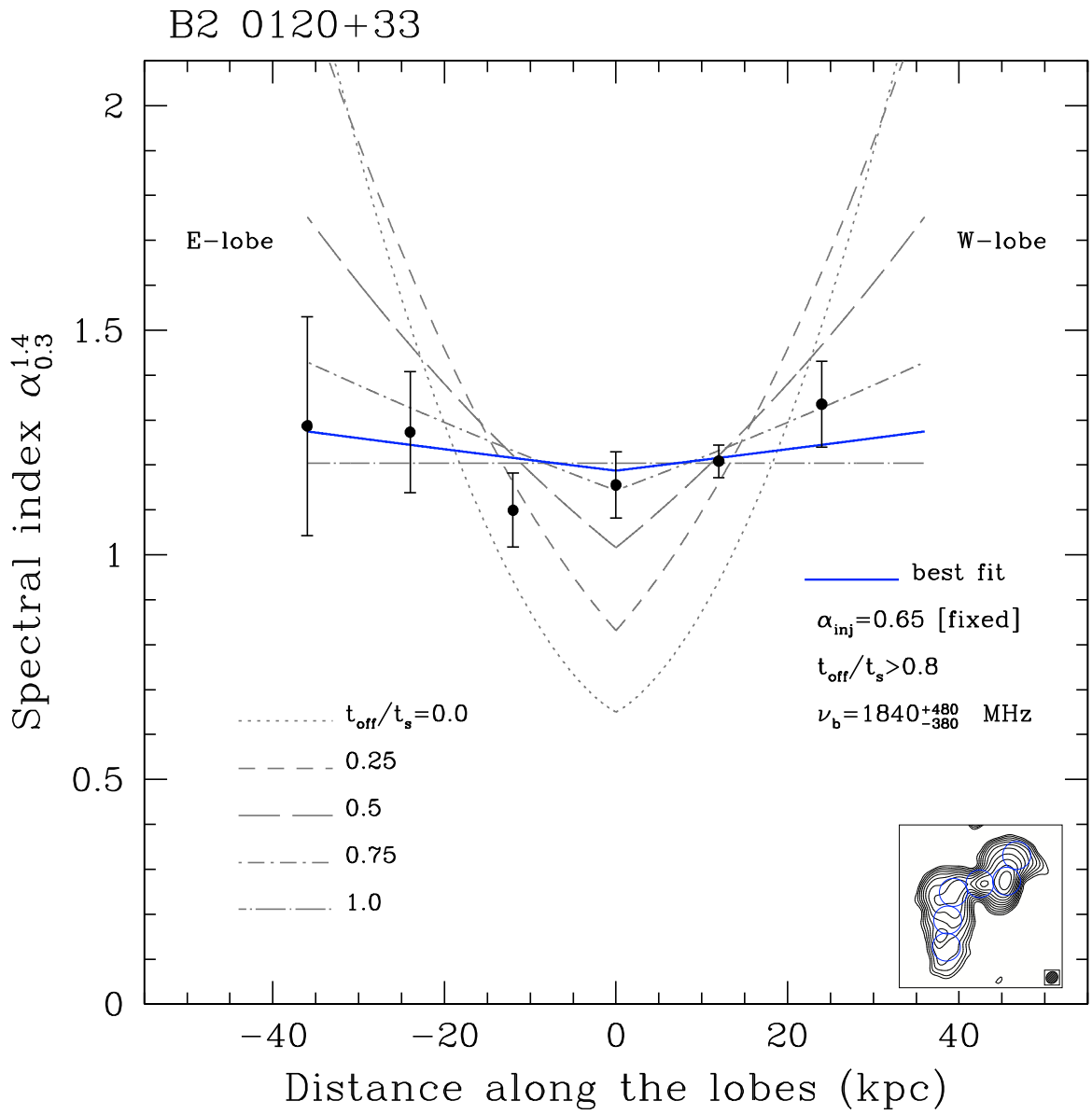

Fig. 7. B2 0120+33 spectral index profile. Each point represents the average over a circular region as shown in the inset. The solid line is the best fit of the CI_{OFF} model described in the text. The reference dashed lines correspond to different relative durations of the dying phase.

high energy ϵ_{high} cut-off is chosen to match the spectral break in the emission spectrum, ν_b, since no electrons are present in the source beyond this limit (see Parma et al. 2007, for further details).

The equipartition parameters computed in this way are reported in Table 6. A comparison with fixed frequency-range calculations shows that the values of our B_{min} are higher by up to a factor two.

5.5. Radiative ages

Assuming a constant magnetic field and neglecting expansion losses, the total source age can be calculated from the break frequency, ν_b

$$t_s = 1590 \frac{B^{0.5}}{(B^2 + B_{IC}^2)[(1+z)\nu_b]^{0.5}}, \quad (8)$$

where the synchrotron age t_s is in Myr, the magnetic field in μG, the break frequency ν_b in GHz, while B_{IC} is the inverse Compton equivalent field (see Sect. 5.2).

By adopting the equipartition value B_{min} for the magnetic field strength, we can thus derive the synchrotron age t_s. Finally, from the ratio t_{OFF}/t_s, which is also given by the fit, we can determine the absolute durations of the active and dying phases, t_{CI} and t_{OFF}. The *total* ages of the five dying sources are on the order of 10^8 yr (with uncertainties up to 50%). For all sources apart from WNB 1829+6911, we are also able to estimate the absolute duration of the active and dying phases that are in the range 10^7–10^8 yr. We note that these numbers should be considered upper limits to the real source ages. It is likely that expansion losses may have played a role in the early stages of the radio source growth, and, in the same manner, the magnetic field strength was presumably higher than the present value. Considering both these effects, the shift of ν_b to low frequencies may have proceeded far more rapidly than expected by the

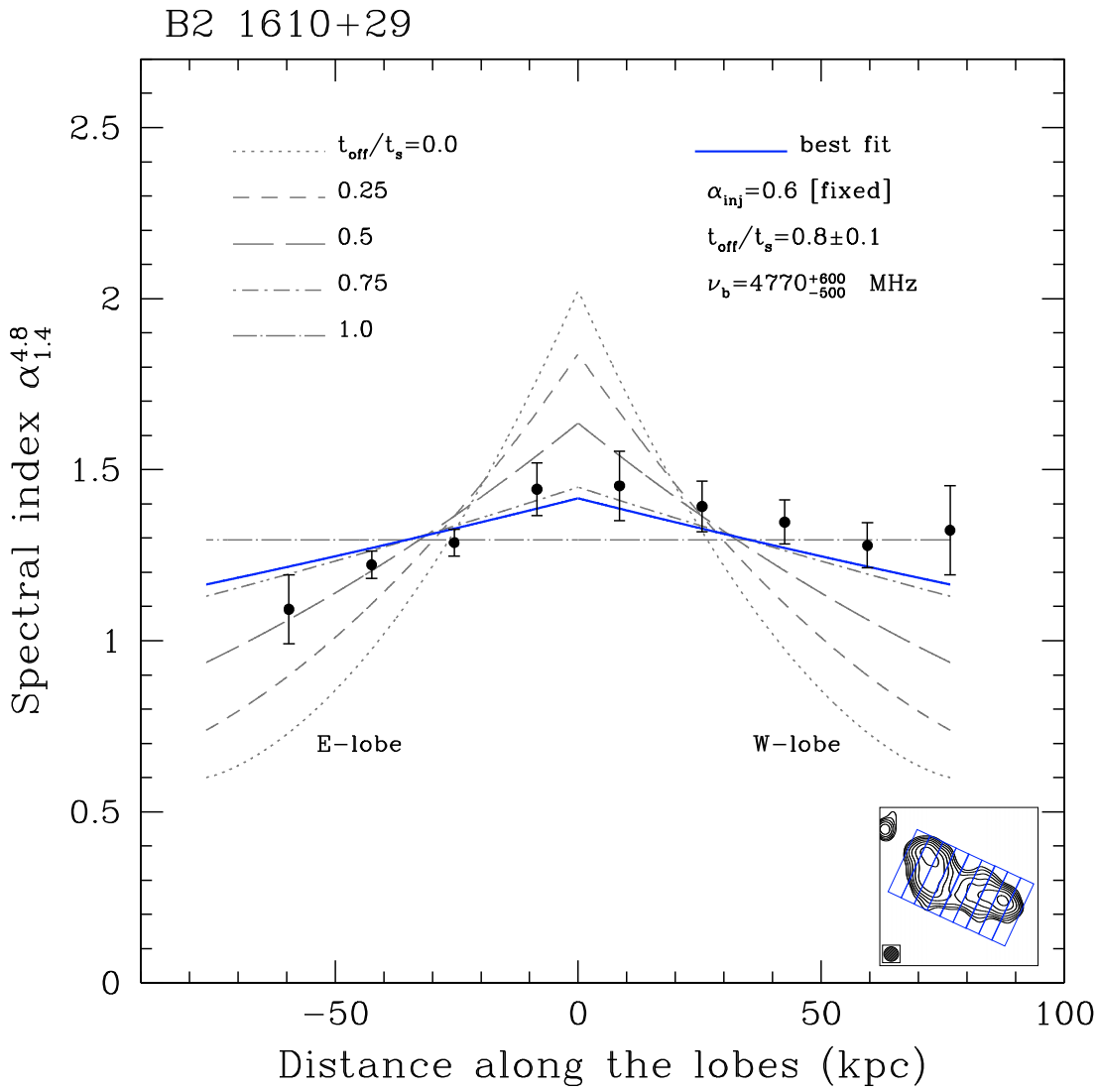

Fig. 8. B2 1610+29 spectral index profile. Each point represents the average over a rectangular region as shown in the inset. The solid line is the best fit of the CI_{OFF} model described in the text. The reference dashed lines correspond to different relative durations of the dying phase.

simple radiative model we considered, and hence the ages would have been overestimated.

6. The X-ray environment

The gaseous environment in which radio galaxies are embedded may play a fundamental role in the later stages of the radio source life. Although no firm conclusions can be drawn about the environment of dying sources, because of the small number of objects involved, it seems that there is a tendency for dying sources to reside in dense environments. Parma et al. (2007) found that about half of the dying sources of their sample are located in clusters of galaxies, while only a few appear to be isolated.

We searched in RASS for possible X-ray counterparts of our five dying radio galaxies. We extracted the 0.1–2.4 keV image of a $15' \times 15'$ field around each radio source. The X-ray images were corrected for the background and smoothed with a $\sigma = 45''$ Gaussian kernel. The RASS count-rate images are shown in Figs. 9 along with the 1.4 GHz VLA C-array iso-contours overlaid. The five dying galaxies presented here do not represent an exception to the rule: each source is located, at least in projection, at the center of an X-ray emitting cluster or galaxy group. The clusters of galaxies are Abell 2276, ZwCl 1829.3+6912, RX J1852.1+5711, ZwCl 0107.5+3212, and Abell 2162 for the radio sources WNB 1734+6407, WNB 1829+6911, WNB 1851+5707, B2 0120+33, and B2 1610+29, respectively.

6.1. Abell 2276

Very little is known about this cluster of galaxies apart from that Jones & Forman (1999) report an X-ray luminosity of 1.02×10^{44} erg/s in the 0.5–4.5 keV band based on *Einstein* data (all X-ray luminosities have been rescaled to our adopted cosmology). The dying source WNB 1734+6407 is associated with the central galaxy at the peak of the X-ray emission (see top-left panel in Fig. 9).

6.2. ZwCl 1829.3+6912

This galaxy cluster is also known as MACS J1829.0+6913 or RX J1829.0+6912. Only sparse information is also present in literature for this cluster. It appears as catalog number NEP5700 in the ROSAT North Ecliptic Pole survey by Gioia et al. (2003).

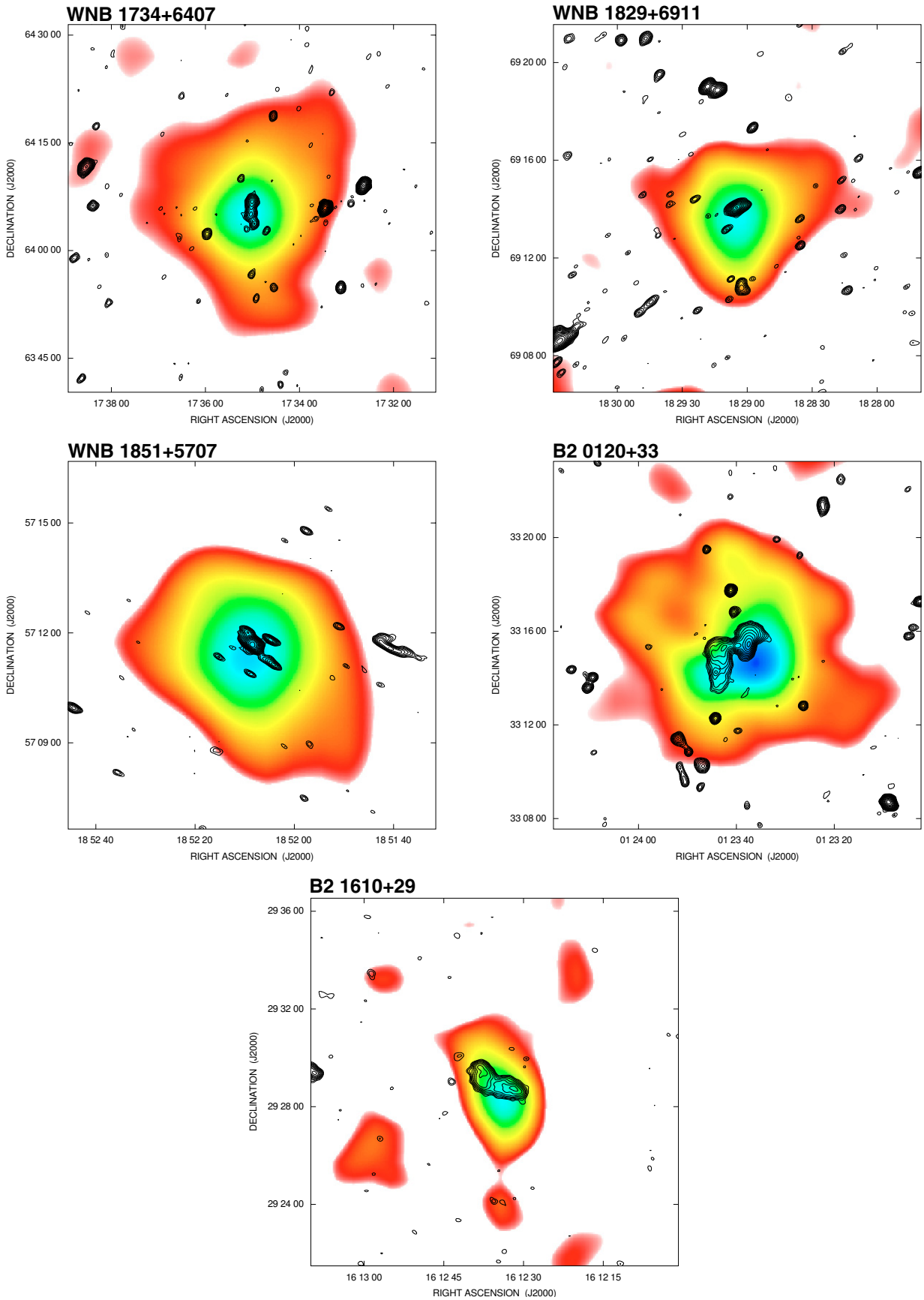

Fig. 9. RASS X-ray images with overlaid the VLA C-array contours at 1.4 GHz. *From top-left to bottom-right*: Abell 2276, ZwCl 1829.3+6912, RXC J1852.1+5711, ZwCl 0107.5+3212, and Abell 2162. Radio contours start from a 3σ rms level and increase in factors of $\sqrt{2}$.

These authors report an X-ray luminosity of 1.06×10^{44} erg/s in the 0.5–2.0 keV band. WNB 1829+6911 is associated with the cD galaxy located close to the X-ray peak (see top-right panel in Fig. 9).

6.3. RX J1852.1+5711

The extended ROSAT Bright Cluster Sample (Ebeling et al. 2000) lists an intrinsic X-ray luminosity in the 0.1–2.4 keV band of 0.95×10^{44} erg/s for this cluster. The dying source WNB 1851+5707a is associated to the galaxy at the center of the X-ray emission, while the dying source WNB 1851+5707b and its host galaxy lie 30″ to the east north. WNB 1851+5707a and WNB 1851+5707b appear blended together at the resolution of the VLA C-array shown as iso-contours in the middle-left panel of Fig. 9.

6.4. ZwCl 0107.5+3212

The dying source B2 0120+33 is identified with the galaxy NGC 507 at the center of the Zwicky cluster 0107.5+3212 and is one of the brightest galaxies in a very dense region. There are 80 galaxies with magnitude $m_{pg} < 15.7$ within a projected distance of 1.5 Mpc from NGC 507. This is the so-called Pisces Group (Parma et al. 1986). The X-ray emission has been studied in detail by many authors with different satellites (see e.g. Kraft et al. 2004, and references therein). NGC 507 is surrounded by an irregular large-scale X-ray emission with a peak coincident with the position of the optical galaxy, and several secondary peaks, caused by the interaction between the radio lobes and the surrounding gas (Paolillo 2003). Kim & Fabbiano (1995) report an X-ray luminosity of 0.8×10^{43} in the 0.1–2.4 keV band for the NGC 507 group. Kraft et al. (2004) observed a sharp edge in the X-ray surface brightness profile in a Chandra observation of NGC 507. These authors suggested that the discontinuity is likely caused by an elemental abundance jump driven by the inflation of the radio lobes and entrainment of material from the central regions of the cluster.

6.5. Abell 2162

Abell 2162 is member of the Hercules cluster super complex (Einasto et al. 2001). The X-ray emission of this nearby cluster of galaxies has been studied by Ledlow et al. (2003), who report an X-ray luminosity in the 0.5–2.0 keV band of 0.16×10^{43} erg/s based on ROSAT data. The fading radio lobes of B2 1610+29 are associated with NGC 6086, the brightest galaxy of the cluster located close to the X-ray peak (Fig. 9 bottom panel).

These results suggest that the occurrence of dying sources could be higher in galaxy clusters, confirming the findings of Parma et al. (2007).

To determine whether the environment really plays a role in increasing either the incidences of or durations of the dying phase, we need to estimate the relative fraction of dying sources in isolated and cluster galaxies. This is not trivial because estimating the completeness of the inhomogeneous radio, optical, and X-ray samples is hard. However, by imposing safer selection limits we can attempt to perform some very rough statistical analysis. A complete sample of 119 sources can be constructed from the minisurvey by considering all galaxies with optical magnitudes $m_r < 16$ and radio flux density $S_{325\ \mathrm{MHz}} > 30$ mJy (de Ruiter et al. 1998). If we restrict our attention to the elliptical galaxies, we have a complete sample of 90 radio sources. We note that we consider WNB 1851+5707 as two distinct radio galaxies, both in the dying phase.

For each of these radio sources, we searched in the NED database for the presence of a galaxy cluster or group to within 10′ from the position of host galaxy. We found that 21 of 90 sources lie, in projection, in Abell, Zwicky, or X-ray selected galaxy clusters or groups, while we considered the rest to be isolated. In this complete sample there are three of our dying sources: WNB 1734+6407, WNB 1851+5707a, and WNB 1851+5707b. The restarting source WNB1829+6911 exceeds the optical limit because of its larger distance and therefore is not included in the complete sample. Therefore, the fraction of dying source in general is ~3.3% (3/90). However, this fraction depends on the environment since the frequency of dying sources in clusters is 14% (3/21).

In the complete B2 bright sample (Colla et al. 1975), we found fossil radio lobes in four of 54 elliptical galaxies. Of these, three (B2 0120+33, B2 1610+29, and B2 1636+39) are in clusters and only one (B2 0924+30) can be considered relatively isolated[5]. By applying the same criterion as described above, we estimated that about 21 radio sources of the B2 sample are located in projection close to the center of a galaxy cluster or group. The fraction of dying source in general is 7% (4/54), while the fraction of dying sources in clusters is 14% (3/21).

The fractions of dying sources (both in general and in clusters) in the minisurvey and in the B2 samples are consistent to within the large uncertainties. We then merged the statistics of the two samples to estimate the probability of a dying source being in cluster:

$$P(\mathrm{cluster}|\mathrm{dying}) = \frac{P(\mathrm{dying}|\mathrm{cluster})P(\mathrm{cluster})}{P(\mathrm{dying})}, \quad (9)$$

where $P(\mathrm{dying}|\mathrm{cluster}) = 6/42$ is the fraction of dying sources in clusters, $P(\mathrm{cluster}) = 42/144$ is the total fraction of radio sources in cluster, and $P(\mathrm{dying}) = 7/144$ is the total fraction of dying sources. We found that the probability of a dying source being in a cluster is $P(\mathrm{cluster}|\mathrm{dying}) = 6/7$, i.e. ~86%. We estimated by means of a simple Monte Carlo simulation that if the probability of there being a dying source were independent of the environment, the probability of having 6/7 dying sources in clusters by chance is less than 0.5%.

One possibility is that the low-frequency radio emission from the fading radio lobes last longer if their expansion is somewhat reduced or even stopped. Another possible explanation is that the frequency of dying sources in clusters is higher. Radio sources in dense environments, such as the centers of cooling core clusters, may have a peculiar accretion mode that results in a bursting duty cycle sequence of active and quiescent periods. Of the five dying galaxies presented in this work, WNB1829+6911 and B2 0120+33 show evidence of a flat-spectrum core. A very faint core is also detected in the MERLIN full-resolution image of WNB1851+5707a, while a steep spectrum feature is detected at the center of the host galaxy of WNB1734+6407. Thus, although the extended fading radio lobes in these sources are not longer powered by kpc-scale jets, the AGN is still radio active at very low levels.

To investigate these hypotheses, we need to compare in detail the actual fading radio structures with the properties of the X-ray emitting gas. We recently observed three of these clusters, Abell 2276, ZwCl 1829.3+6912, and RXC J1852.1+5711, with the Chandra satellite. We will report the results of these observations in a forthcoming paper (Murgia et al., in prep.).

[5] The dying source B2 0924+30 is a member of the nearby poor cluster WBL224 (White et al. 1999), but no extended X-ray emission is present in the RASS.

7. Summary

We have presented the study of five "dying" radio galaxies belonging to the Westerbork Northern Sky Survey minisurvey and to the B2 bright sample: WNB1734+6407, WNB1829+6911, WNB1851+5707, B2 0120+33, and B2 1610+29.

These sources have been selected on the basis of their extremely steep broad-band radio spectra, which is a strong indication that these objects either belong to the rare class of dying radio galaxies or that we are observing "fossil" radio plasma remaining from previous nuclear activity. We derived the relative duration of the dying phase from the fit of a synchrotron radiative model to the radio spectra of the sources. The modeling of the integrated spectra and the deep spectral index images obtained with the VLA confirmed that in these sources the central engine has ceased to be active for a significant fraction of their lifetime, although their extended lobes have not yet completely faded away. In the cases of WNB1829+6911 and B2 0120+33, the fossil radio lobes are seen in conjunction with a currently active core. We found that WNB1851+5707 is in reality composed of two distinct dying sources that originally appeared blended together at the lower angular resolution of the WENSS.

All the dying sources of our sample are located (at least in projection) at the center of an X-ray emitting cluster.

Although no firm conclusions can be drawn because of the small number statistics involved, our results suggest that the duration of the dying phase of a radio sources in a cluster can be significantly higher than that of a radio galaxy in the field. The simplest interpretation for the tendency of dying galaxies to be found in clusters is that the low-frequency radio emission from the fading radio lobes lasts longer if their expansion is somewhat reduced or even stopped by the pressure of a particularly dense intra-cluster medium. Another possibility is that the occurrence of dying sources is higher in galaxy clusters. Of the five dying galaxies, WNB1829+6911 and B2 0120+33 show evidence of a flat-spectrum core. A very faint core is also detected in the MERLIN full-resolution image of WNB1851+5707a, while a steep spectrum feature is detected at the center of the host galaxy of WNB1734+6407. Thus, although the extended fading radio lobes in these sources are no longer powered by kpc-scale jets, the AGN is still radio active at very low levels. This suggests that radio sources in dense environments, such as the centers of cooling core clusters, have a peculiar accretion mode that results in a bursting duty cycle sequence of active and quiescent periods. This result could have important implications for theories of the life cycles of radio sources and AGN feedback in clusters of galaxies but awaits confirmation from future observations of larger, statistically significant, samples of objects.

A large fraction of dying radio sources may have been missed by the current surveys because of their very steep spectra. These sources are very faint at centimeter wavelengths but should still be visible at frequencies below 100 MHz if they are only subject to radiative losses. Owing to their high sensitivity and angular resolution, the upcoming low-frequency radio interferometers (such as LOFAR and LWA and, in the near future, SKA) represent the ideal instruments to discover and study in detail these elusive objects.

Acknowledgements. We are grateful to the anonymous referee for very useful comments that improved this paper. FG and MM thank the hospitality of the Harvard-Smithsonian Center for Astrophysics where part of this research was done. Support was provided by Chandra grant GO9-0133X, NASA contract NAS8-39073, and the Smithsonian Institution. We acknowledge financial contribution from the agreement ASI-INAF I/009/10/0. The National Radio Astronomy Observatory is operated by Associated Universities, Inc., under contract with the National Science Foundation. This research made use of the NASA/IPAC Extragalactic Database (NED) which is operated by the Jet Propulsion Laboratory, California Institute of Technology, under contract with the National Aeronautics and Space Administration. MERLIN is a National Facility operated by the University of Manchester at Jodrell Bank Observatory on behalf of STFC. This work has benefited from research funding from the European Community's sixth Framework Programme under RadioNet R113CT 2003 5058187. This research made use also of the CATS Database (Astrophysical CATalogs support System). The optical DSS2 red images were taken from: http://archive.eso.org/dss/dss. We thank the staff of the National Galileo Telescope (TNG) for carrying out the optical observations in service mode.

References

Altieri, F., et al. 1999, Laurea Thesis, University of Bologna
Baars, J. W. M., Genzel, R., Pauliny-Toth, I. I. K., & Witzel, A. 1977, A&A, 61, 99
Beck, R., & Krause, M. 2005, Astron. Nachr., 326, 414
Brunetti, G., Setti, G., & Comastri, A. 1997, A&A, 325, 898
Cohen, A. S., Lane, W. M., Cotton, W. D., et al. 2007, AJ, 134, 1245
Colla, G., Ficarra, A., Formiggini, L., et al. 1970, A&AS, 1, 281
Colla, G., Fanti, C., Fanti, R., et al. 1972, A&AS, 7, 1
Colla, G., Fanti, C., Fanti, R., et al. 1973, A&AS, 11, 291
Colla, G., Fanti, C., Fanti, R., et al. 1975, A&A, 38, 209
Condon, J. J., Cotton, W. D., Greisen, E. W., et al. 1998, AJ, 115, 1693
Cordey, R. A. 1987, MNRAS, 227, 695
Douglas, J. N., Bash, F. N., Bozyan, F. A., et al. 1996, AJ, 111, 1945
Dressel, L. L., & Condon, J. J. 1978, ApJS, 36, 53
Ebeling, H., Edge, A. C., Allen, S. W., et al. 2000, MNRAS, 318, 333
Einasto, M., Einasto, J., Tago, E., Müller, V., & Andernach, H. 2001, AJ, 122, 2222
Fanaroff, B. L., & Riley, J. M. 1974, MNRAS, 167, 31P
Feretti, L., & Giovannini, G. 1980, A&A, 92, 296
Ferrari, C., Govoni, F., Schindler, S., et al. 2008, Space Sci. Rev., 134, 93
Gentile, G., Rodríguez, C., Taylor, G. B., et al. 2007, ApJ, 659, 225
Giacintucci, S., Venturi, T., Murgia, M., et al. 2007, A&A, 476, 99
Gioia, I. M., Henry, J. P., Mullis, C. R., et al. 2003, ApJS, 149, 29
Giovannini, G., Feretti, L., Gregorini, L., & Parma, P. 1988, A&A, 199, 73
Helmboldt, J. F., Kassim, N. E., Cohen, A. S., et al. 2008, ApJS, 174, 313
Hales, S. E. G., Masson, C. R., Warner, P. J., & Baldwin, J. E. 1990, MNRAS, 246, 256
Hales, S. E. G., Mayer, C. J., Warner, P. J., & Baldwin, J. E. 1991, MNRAS, 251, 46
Hales, S. E. G., Baldwin, J. E., & Warner, P. J. 1993, MNRAS, 263, 25
Hales, S. E. G., Waldram, E. M., Rees, N., & Warner, P. J. 1995, MNRAS, 274, 447
Jamrozy, M., Klein, U., Mack, K.-H., Gregorini, L., & Parma, P. 2004, A&A, 427, 79
Jones, D. L., & Preston, R. A. 2001, AJ, 122, 2940
Kim, D. W., & Fabbiano, G. 1995, ApJ, 441, 182
Komissarov, S. S., & Gubanov, A. G. 1994, A&A, 285, 27
Kraft, R. P., Forman, W. R., Churazov, E., et al. 2004, ApJ, 601, 221
Ledlow, M. J., Voges, W., Owen, F. N., & Burns, J. O. 2003, AJ, 126, 2740
Liuzzo, E., Giovannini, G., Giroletti, M., & Taylor, G. B. 2010, A&A, 516, A1
Murgia, M., Fanti, C., Fanti, R., et al. 1999, A&A, 345, 769
Pacholczyk, A. G. 1970, Series of Books in Astronomy and Astrophysics (San Francisco: Freeman)
Paolillo, M., Fabbiano, G., Peres, G., & Kim, D.-W. 2003, ApJ, 586, 850
Parma, P., de Ruiter, H. R., Fanti, C., & Fanti, R. 1986, A&AS, 64, 135
Parma, P., Murgia, M., Morganti, R., et al. 1999, A&A, 344, 7
Parma, P., Murgia, M., de Ruiter, H. R., et al. 2007, A&A, 470, 875
Rengelink, R. B., Tang, Y., de Bruyn, A. G., et al. 1997, A&AS, 124, 259
Riley, J. M. 1989, MNRAS, 238, 1055
de Ruiter, H. R., Parma, P., Stirpe, G. M., et al. 1998, A&A, 339, 34
Saripalli, L., Subrahmanyan, R., & Udaya Shankar, N. 2002, ApJ, 565, 256
Saripalli, L., Subrahmanyan, R., & Udaya Shankar, N. 2003, ApJ, 590, 181
Scheuer, P. A. G. 1974, MNRAS, 166, 513
Schoenmakers, A. P., de Bruyn, A. G., Röttgering, H. J. A., & van der Laan, H. 2000, MNRAS, 315, 395
Slee, O. B., Roy, A. L., Murgia, M., et al. 2001, AJ, 122, 1172
Sohn, B. W., Klein, U., & Mack, K.-H. 2003, A&A, 404, 133
Verkhodanov, O. V., Trushkin, S. A., Andernach, H., & Chernenkov, V. N. 1997, Astronomical Data Analysis Software and Systems VI, 125, 322
White, R. A., Bliton, M., Bhavsar, S. P., et al. 1999, AJ, 118, 2014
Zhang, X., Zheng, Y., Chen, H., et al. 1997, A&AS, 121, 59